Paleoceanography and Paleoclimatology

AGU ADVANCING EARTH AND SPACE SCIENCE

RESEARCH ARTICLE
10.1029/2021PA004386

The Origin of Tree-Ring Reconstructed Summer Cooling in Northern Europe During the 18th Century Eruption of Laki

Julie Edwards[1,2], Kevin J. Anchukaitis[1,2], Björn E. Gunnarson[3], Charlotte Pearson[2], Kristina Seftigen[4,5], Georg von Arx[5,6], and Hans W. Linderholm[4]

[1]School of Geography, Development, and Environment, University of Arizona, Tucson, AZ, USA, [2]Laboratory of Tree-Ring Research, University of Arizona, Tucson, AZ, USA, [3]Department of Physical Geography, Stockholm University, Stockholm, Sweden, [4]Department of Earth Sciences, University of Gothenburg, Gothenburg, Sweden, [5]Swiss Federal Institute for Forest Snow and Landscape Research WSL, Birmensdorf, Switzerland, [6]Oeschger Centre for Climate Change Research, University of Bern, Bern, Switzerland

Key Points:

- High-resolution tree ring density measurements provide approach for identifying extreme environmental events
- The normal climate/MXD relationship is disrupted or obfuscated by the consequences of what is most likely the direct effects of acidic haze
- Screening anatomical series for anomalies can lead to an evaluation of potentially confounding factors for climate reconstructions

Correspondence to:
J. Edwards,
julieedwards@email.arizona.edu

Citation:
Edwards, J., Anchukaitis, K. J., Gunnarson, B. E., Pearson, C., Seftigen, K., von Arx, G., & Linderholm, H. W. (2022). The origin of tree-ring reconstructed summer cooling in northern Europe during the 18th century eruption of Laki. *Paleoceanography and Paleoclimatology*, *37*, e2021PA004386. https://doi.org/10.1029/2021PA004386

Received 9 NOV 2021
Accepted 19 JAN 2022

Abstract Basaltic fissure eruptions, which are characteristic of Icelandic volcanism, are extremely hazardous due to the large quantities of gases and aerosols they release into the atmosphere. The 1783–1784 CE Laki eruption was one of the most significant high-latitude eruptions in the last millennium and had substantial environmental and climatic impacts. Contemporary observations recorded the presence of a sulfuric haze over Iceland and Europe, which caused famine from vegetation damage and resulted in a high occurrence of respiratory illnesses and related mortality. Historical records in northern Europe show that the summer of 1783 was anomalously warm, but regional tree-ring maximum latewood density (MXD) data from that year are low and lead to erroneously colder reconstructed summer temperatures. Here, we measure wood anatomical characteristics of Scots pine (*Pinus sylvestris*) from Jämtland, Sweden in order to identify the cause of this discrepancy. We show that the presence of intraannual density fluctuations in the majority of 1783 growth rings, a sudden reduction in lumen and cell wall area, and the measurement resolution of traditional X-ray densitometry led to the observed reduced annual MXD value. Multiple independent lines of evidence suggest these anatomical anomalies were most likely the result of direct acidic damage to trees in Northern Europe and that the normal relationship between summer temperature and MXD can be disrupted by this damage. Our study also demonstrates that quantitative wood anatomy offers a high-resolution approach to identifying anomalous years and extreme events in the tree-ring record.

1. Introduction

More than 800 million people live within 100 km of an active volcano and may therefore potentially be exposed to health and environmental hazards from eruptions (Brown et al., 2015; Hansell & Oppenheimer, 2004). Basaltic fissure eruptions, which are characteristic of Icelandic volcanism, are particularly hazardous due to the large quantities of gases and aerosols released into the atmosphere (Carlsen et al., 2021; Thordarson & Larsen, 2007) and simulations of the health consequences of volcanic air pollution confirm that future events pose a considerable risk to the United Kingdom and Europe (Carlsen et al., 2021; Dawson et al., 2021; Schmidt, 2015; Schmidt et al., 2011). Icelandic eruption aerosols may also cause a decrease in temperatures or reduction of incoming solar radiation, causing widespread reductions in agricultural yields, as was observed during the 939–940 CE Eldgjá eruption (Oppenheimer et al., 2018). More recently, even the comparatively small 2010 CE Eyjafjallajökull and the 2011 CE Grímsvötn eruptions impeded air travel and caused economic disruption across Europe and the North Atlantic (Budd et al., 2011; Gudmundsson et al., 2012; Oppenheimer, 2015; Schmidt, 2015). These two modern eruptions and the 2014 CE–2015 CE Holuhraun eruption also caused detrimental respiratory health effects (Carlsen et al., 2012, 2021; Damby et al., 2017). Over the entirety of the Common Era however, the 939–940 CE Eldgjá and 1783–1784 CE Laki (Lakagígar) eruptions have thus far had the most significant environmental and climatic impacts. The Laki eruption was one of the largest, in terms of the mass of SO_2 emitted, high-latitude eruptions of the last millennium (Sigl et al., 2015; Thordarson & Larsen, 2007) and among the most deadly of the last 400 years (Auker et al., 2013). The study of Common Era Icelandic eruptions provides perspective on the potential hazards and impacts of future events.

The 1783–1784 Laki eruption is particularly interesting because it coincided with a period of extreme and unusual weather and atmospheric phenomena across Europe. The Laki eruption sequence began in 8 June 1783 and did not

end until 7 February 1784, emitting an estimated 122 megatons SO_2 into the atmosphere (Thordarson & Self, 2003). Contemporary observations establish both the occurrence of a "haze" across Europe and an abnormal heat wave in Western and Central Europe during the summer of 1783 (Franklin, 1785; Grattan & Charman, 1994; Grattan & Pyatt, 1999; Grattan & Sadler, 1999; Luterbacher et al., 2004; Stothers, 1996; Thordarson & Self, 1993, 2003). This opaque dry haze in the lower troposphere, comprised mostly of sulfuric acid (H_2SO_4), was observed across much of Europe by 26 June, and while the last known appearance of this haze is ambiguous it is likely to have been late in October of 1783 (Oman et al., 2006; Thordarson & Self, 2003). Modeling experiments show high surface sulfate aerosol concentrations averaged over the longitude band from 24.48°W (Iceland) to 5.68°E (Western Europe) centered around 65°N throughout the summer of that year (Chenet et al., 2005). The warm summer temperatures were intensified by anomalously high pressure and atmospheric blocking over Europe, which would have also contributed to a more persistent haze (Thordarson & Self, 2003; Zambri et al., 2019a). Retrospective studies have shown that the synoptic atmospheric configuration at the time of the eruption could be considered the worst-case scenario in terms of bringing volcanic pollution to Europe (Dawson et al., 2021). The haze, also referred to as a "dry fog," lead to widespread respiratory illnesses across Europe (Durand & Grattan, 1999; Grattan et al., 2003; Witham & Oppenheimer, 2004). A Laki-like eruption today would be a severe health and environmental hazard across Europe (Schmidt, 2015; Schmidt et al., 2011; Sonnek et al., 2017).

While summer cooling due to the reduction of incoming solar radiation is the expected and frequently observed climate response to large and sulfur-rich volcanic eruptions (Robock, 2000; Timmreck, 2012), early instrumental and documentary historical records actually show that the summer of 1783 was abnormally warm throughout much of Europe, including Sweden (Luterbacher et al., 2004; Thordarson & Self, 2003). This time frame coincides with when models show peak sulfate loading in the upper troposphere/lower stratosphere (Oman et al., 2006; Zambri et al., 2019b). The summer heatwave has been associated with the presence of a high pressure air mass, and written records associate the hottest days of this period with the thickest occurrences of the Laki haze (Thordarson & Self, 2003). It has been suggested that the haze may also have played a role in exacerbating localized warming (Grattan & Sadler, 1999). Tree-ring data are often used to reconstruct the climate consequences of past volcanic eruptions and maximum latewood density (MXD) is considered to be the most accurate metric for quantifying volcanic climate signals (Anchukaitis et al., 2017; Björklund et al., 2019; D'Arrigo et al., 2013; Esper et al., 2015, 2018; Frank et al., 2007; Stoffel et al., 2015; Wilson et al., 2016). Contrary to the historical record, however, temperature reconstructions that use MXD indicate widespread cooling over much of Europe in the summer of 1783 (Anchukaitis et al., 2017; Edwards et al., 2021; Guillet et al., 2017; Hakim et al., 2016; Luterbacher et al., 2016; Tardif et al., 2019; Tingley & Huybers, 2013). As an example, the Luterbacher et al. (2004) reconstruction used predominantly historical, documentary, and early instrumental data to estimate past temperatures and thus shows the warming over much of northern Europe, including Sweden, in 1783. However, the more recent Luterbacher et al. (2016) reconstruction uses predominantly tree-ring data over this region, and shows cooling in 1783 (Figure 1). Previous authors have speculated this inconsistency—which is seen in most tree-ring reconstructions (Edwards et al., 2021)—might be the direct result of the volcanic eruption on European tree growth (Briffa et al., 1988; Jones et al., 1995; Schove, 1954). While weather conditions across Europe were variable throughout the summer of 1783 (it was, for instance, indeed unusually cold in Iceland) (Thordarson & Self, 2003), here we are specifically concerned with the discrepancies between the tree-ring reconstructed cooling and the observed warming recorded over Northern Europe. In this study, we use new quantitative wood anatomy analyses, historical temperature data, and existing tree-ring carbon isotope data to investigate the origin of this discrepancy between the tree-ring temperature proxy data and 18th century weather observations. By investigating this difference, we seek to more fully understand the European environmental impacts of the eruption, provide information on the potential biological effects of future Icelandic fissure eruptions, and address the paleoclimate implications of the direct impacts of extreme events on tree-ring proxy data.

2. Methods and Data

2.1. Quantitative Wood Anatomy

Both living and preserved dead (subfossil) samples of Scots pine (*Pinus sylvestris*) were collected just east of the Scandinavian Mountains in Jämtland (Sweden) to produce an updated C-Scan (central Scandinavia) chronology (63.30°N, 13.25°E; Figure 2), herein identified as CSCAN2019 (Linderholm & Gunnarson, 2019; Zhang et al., 2016). Jämtland is one of several Fennoscandian and northwestern Siberia tree-ring density chronologies,

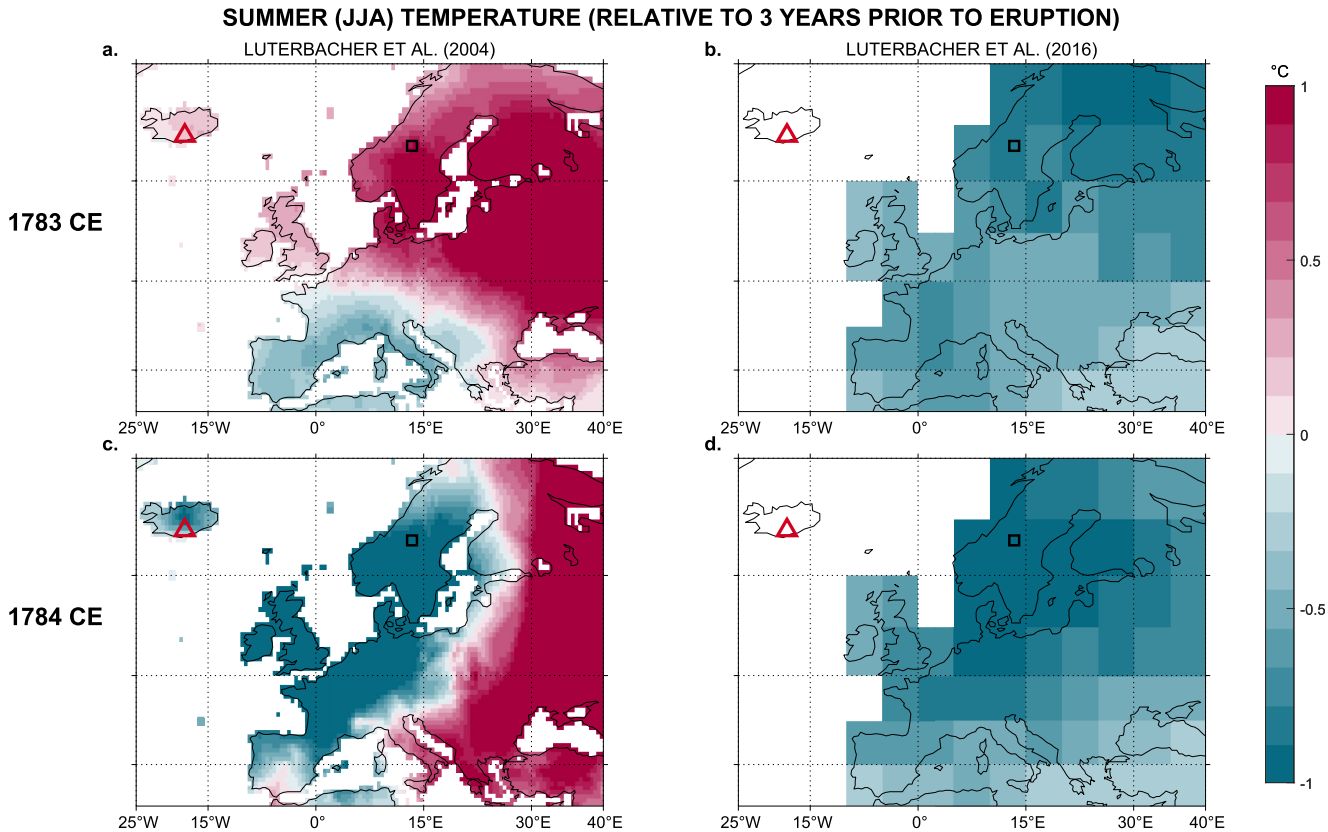

Figure 1. Proxy reconstructed summer (June through August) mean temperature anomalies in 1783 CE from (a), Luterbacher et al. (2004) and (b), Luterbacher et al. (2016), and in 1784 CE from (c), Luterbacher et al. (2004) and (d), Luterbacher et al. (2016), relative to the mean temperature of the 3 years prior to the Laki eruption. The red triangle marks the location of the Laki volcano and the black square marks the location of the Jämtland study site. The positive temperature anomaly in (a) is dominated by the use of historical, documentary, and early instrumental data. Panel (b) is created mostly from tree-ring proxy data, including maximum latewood density (MXD) at the Jämtland site (Gunnarson et al., 2011). Other temperature field reconstructions using a wide range of proxy observations and statistical methods also show cooling over Northern Europe in 1783 (see Figure 1 in Edwards et al., 2021) (e.g., Anchukaitis et al., 2017; Guillet et al., 2017; Tardif et al., 2019; Tingley & Huybers, 2013).

including also the Polar Urals, Kola Peninsula, Yamal, and Forfjorddalen, that contribute to reconstructed cold temperature anomalies across northern Europe region in 1783 (Anchukaitis et al., 2017; Wilson et al., 2016). Most importantly, Jämtland is also relatively close to several 18th century historical climate data records that can be used for comparison with the proxy record (see Section 2.2). There is also an existing tree-ring carbon isotope chronology in Jämtland at Furuberget (see Section 2.3). From the existing CSCAN2019 collection, we selected nine samples for quantitative wood anatomy analysis (QWA; von Arx et al., 2016) that spanned the full period from 1768 to 1798. The majority of the samples chosen were mature (>50 years old) at the time of the Laki eruption, while three were juvenile (<33 years old). The crossdated chronology, ring-width measurements, and MXD series were previously developed following standard dendrochronological procedures (Linderholm & Gunnarson, 2019). The original MXD data were measured using an Itrax Multiscanner (Cox Analytical Systems) with the opening width of the sensor slit set to 20 µm at each step (Linderholm & Gunnarson, 2019). We used the original raw TRW measurements to verify the dating of the nine samples used here prior to processing the cores for QWA analysis. For this study, we also created a Jämtland TRW chronology by fitting a cubic smoothing spline with 50% frequency response cutoff at 30 years to a selection of raw ring width measurements using the R-package dplR (Bunn, 2008; R Core Team, 2019).

We cut the wood samples to a thickness of 10 µm using a rotary microtome (Microm HM355S). The wood microsections were stained with a safranin solution, permanently fixed in Eukitt, and prepared following standard procedures (Gärtner & Schweingruber, 2013; von Arx et al., 2016). Digital images of the microsections were produced at the Swiss Federal Research Institute WSL in Birmensdorf, Switzerland, using a Zeiss Axio Scan Z1. We measured the cell lumen area, cell wall thickness, and cell wall area for the period 1768 to 1798 on all samples

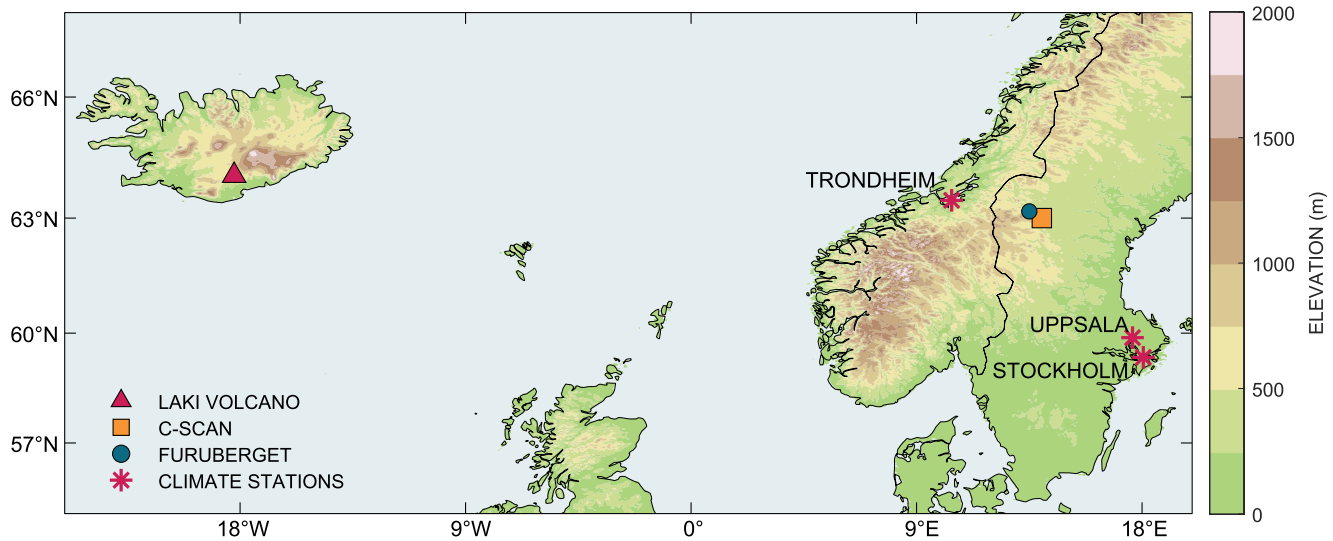

Figure 2. Map of locations relevant to this study. C-Scan (orange square) is the general area of the Jämtland (Sweden) sampling sites where the *Pinus sylvestris* samples used in this study were collected. Furuberget (blue circle) is the sampling site from Seftigen et al. (2011) where tree-ring carbon isotope data covering the eruption period are available. The mapped location of the Trondheim climate station (pink asterisk) is the approximate average location between the Trondheim/Tyholt and Trondheim/Vaernes stations.

using the ROXAS (v3.1) image analysis software (Prendin et al., 2017; von Arx & Carrer, 2014). We excluded measurements of samples with cell walls damaged during sampling or preparation. A total of 452,056 tracheid cells were measured for the 30-year period. To create radial profiles of cell measurements for analysis, we used a locally weighted smoothing (LOWESS) regression with a 10% span to fit curves to the anatomical measurements (Cleveland, 1979). Confidence intervals around each curve were estimated from the residuals of the lowess fit. Although the eruption and its environmental consequences did continue into 1784 (D'Arrigo et al., 2011; Zambri et al., 2019b), for this study we consider 1783 the "Laki year" and we use the remaining 30 years of wood anatomical data as a "control" to provide context for growth anomalies in 1783.

We calculated anatomical MXD (aMXD) as the maximum ratio between the cell wall area and the full tracheid area (the sum of the cell wall area and cell lumen area) for any given year at a range of measurement resolutions. We used the same series of 10–160 µm resolutions used by Björklund et al. (2019) to simulate those of other common density measurement techniques. To calculate the 10 µm resolution values of a single year, for example, the raw cellular measurements are assigned 10 µm wide bands parallel to the ring borders (Björklund et al., 2020). Then, the median value of all cells within each respective band is used as the representative value for that band. If the last band is less than 10 µm then it is defined as the 10 µm adjacent to the terminal ring border (Björklund et al., 2020). For aMXD as with traditional MXD, a single value is therefore calculated for each ring. The average aMXD of the nine cores were used to create an ensemble of multiple resolution aMXD chronologies. A number of studies have now shown that detrending may not be necessary for some anatomical data (Björklund et al., 2020; Carrer et al., 2018; Liang et al., 2013). We calculated the Pearson correlation coefficient between the original CSCAN2019 MXD chronology and each aMXD chronology from 1768 to 1798. We also applied a Mann–Kendall test ($\alpha = 0.05$) to the TRW, MXD, and aMXD chronologies to identify any significant trends.

Intraannual wood density fluctuations (IADFs) in the annual rings were identified both visually and using an automatic statistical detection approach. For visual identification, we used the classifications described in Campelo et al. (2007) and specifically looked for earlywood-like cells in the middle of the latewood (IADF L) and earlywood-like cells at the very end of the latewood (IADF L+). The same microsection images used to produce the quantitative wood anatomy data were used for visual IADF identification (Figure 3). For automatic detection of IADFs, we leveraged the increase in lumen area in latewood that is caused by IADFs. We first created tracheidograms (Vaganov, 1990), standardized to 100 cells, of lumen area for each core from 1768 to 1798. Then, we applied a 10-cell Gaussian smoothing filter to the standardized tracheidograms. Years with an IADF were then defined by a peak in the smoothed lumen area tracheidogram in the last 20% of the ring.

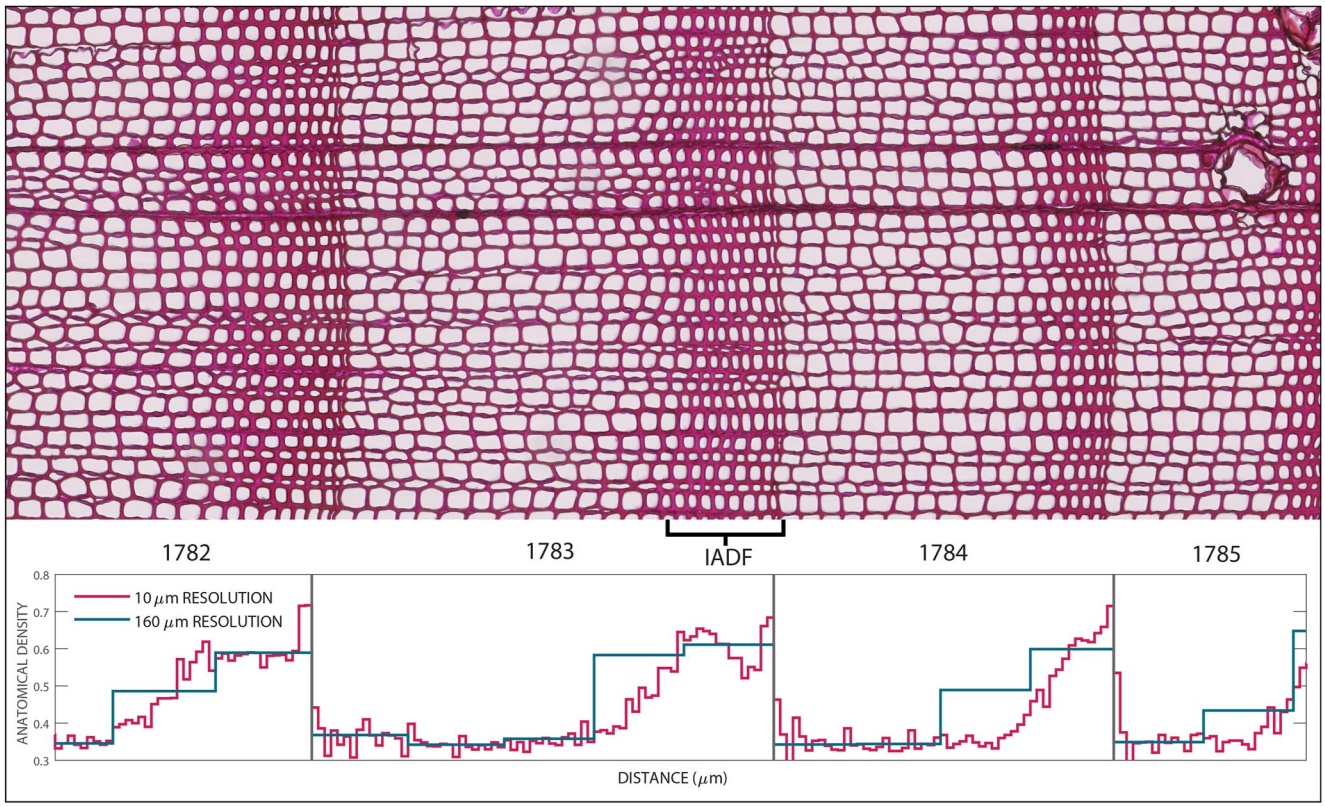

Figure 3. Example micrograph of Scots pine sample Fb06_26a from Jämtland, stained with safranin. An intraannual density fluctuation (IADF) can be seen in the 1783 ring. Earlywood to latewood growth is shown going from left to right. Raw values of intraannual measurements of anatomical density taken at 10 and 160 μm resolution are plotted at their approximate location within each annual ring.

2.2. Climate Data

In order to evaluate the climate signal contained in wood anatomy and wood density series from the 18th century, as well as the potential for short-term weather fluctuations to affect wood anatomy (e.g., Piermattei et al., 2020), we retrieved historical average monthly adjusted temperature data for the Uppsala (59.88°N, 17.62°E, 27 m a.s.l.), Trondheim/Vaernes (63.50°N, 10.90°E, 12 m a.s.l.), and Trondheim/Tyholt (63.41°N, 10.45°E, 122 m a.s.l.) climate stations from the Berkeley Earth compilation (BEST; Lawrimore et al., 2011; Menne et al., 2018; Rohde & Hausfather, 2020). The Uppsala station is nearly 500 km away from the Jämtland sampling site and the Trondheim stations are located on the west side of the Scandinavian mountains, where climate differs from Jämtland. To estimate the relationship between climate at the Jämtland sampling site and Uppsala and Trondheim, we also retrieved modern average monthly temperature data for the nearby Östersund (63.16°N, 14.40°E, 367 m a.s.l.) and Höglekardalen (63.08°N, 13.75°E, 592 m a.s.l.) climate stations from the Berkeley Earth compilation (BEST; Lawrimore et al., 2011; Menne et al., 2018; Rohde & Hausfather, 2020). We averaged the data from the Trondheim/Vaernes and the Trondheim/Tyholt stations due to their proximity (25 km distance) and similarity ($r = 0.99$ for the 1768–1798 period), and to compensate for missing values in each record. We calculated the Pearson correlation coefficient between the monthly data at both climate stations and the multiple resolution aMXD and CSCAN2019 MXD chronologies from 1768 to 1798. We also retrieved historical homogenized and adjusted daily mean temperature data for Stockholm (59.35°N, 18.05°E) from the Bolin Centre Database (Moberg, 2020). Summer temperatures in that series have been adjusted to account for a previously identified warm bias in the observations (Moberg, 2020).

2.3. Carbon Isotope Data

Here, we use the existing $\delta^{13}C$ record of Scots pine from the Furuberget site in the central Scandinavian Mountains (63.17°N, 13.50°E—Figure 2) as an additional environmental proxy to compare against the MXD chronologies

(Seftigen et al., 2011). This δ^{13}C series was previously found to have a strong positive correlation with summer temperatures from 1901 to 2000 across Jämtland and eastern Norway (Seftigen et al., 2011). We subtracted 3‰ from the δ^{13}C series to account for the conversion of leaf carbohydrate to wood, and then converted this leaf-corrected δ^{13}C to isotopic discrimination (Δ^{13}C) using Equation (1) (Belmecheri & Lavergne, 2020; Leavitt & Long, 1982; Mathias & Thomas, 2018).

$$\Delta^{13}C = \left(\frac{\delta^{13}C_{air} - \delta^{13}C_{plant}}{1 + \frac{\delta^{13}C_{plant}}{1{,}000}} \right) \quad (1)$$

For $\delta^{13}C_{air}$ we used $\delta^{13}CO_2$ compiled by Belmecheri and Lavergne (2020), who interpolated pre-1850 $\delta^{13}CO_2$ annual values using the Bauska et al. (2015) and Eggleston et al. (2016) reconstructions. We calculated the Pearson correlation coefficient between Δ^{13}C and the multiple resolution aMXD and CSCAN2019 MXD chronologies from 1768 to 1798, both including and excluding the post-eruption years 1783, 1784, and 1785.

2.4. X-Ray Fluorescence

We conducted X-ray fluorescence (XRF) analysis on three tree-ring core samples in order to test for the presence of a potential dendrochemical response from the impact of the acidic haze. Two trees were young (<33 years old) and one tree was mature (>100 years old) at the time of the eruption. These three cores were also used for QWA analysis. Tree rings can be promising targets for detecting sulfur pollution and may be used to identify volcanic events (Binda et al., 2021; Fairchild et al., 2009; Hevia et al., 2018; Pearson et al., 2005, 2009). Because sulfur is structurally fixed in the wood, it can be a reliable indicator of environmental pollution (Fairchild et al., 2009). However, the final amount of sulfur in the woody tissue is affected by the different sources and pathways to the tree. Pine needles take up sulfur directly from the atmosphere whereas nutrients for wood growth come from soil water, which are additionally subject to site conditions like soil alkalinity (Fairchild et al., 2009; Hevia et al., 2018). XRF is nondestructive while providing detection of multiple different elements and has an adjustable spatial resolution (Smith et al., 2008). We carried out XRF analysis using IXRF System's Atlas Micro-XRF unit, making a series of area scans of approximately 3 mm wide by 10 mm long with a point dwell of 800 µs at 20 micron resolution. The primary excitation source was 50 kV/50 W/1 mA with a Rh target. The instrument uses X-rays to excite the surface of the sample, which produces characteristic X-rays that are at measurable energies specific to the elements present. By moving the sample under the X-ray source at regular intervals, a map of relative elemental abundances on the core surface is produced (Pearson et al., 2020).

3. Results

3.1. Quantitative Wood Anatomy

The original complete TRW chronology (N = 24 cores; Linderholm & Gunnarson, 2019) and the average raw TRW of our QWA subset (N = 9 cores) are significantly and positively correlated over their common interval (1768–1798, r = 0.65, p < 0.01; Figure 4a). Both show a sharp decrease in ring width after 1783. Based on our Mann–Kendall test, the raw TRW series of our QWA subset has a significant downward trend over the period 1768 to 1798 CE, which is likely in part an age-related growth effect, while none of the aMXD chronologies have a significant trend. The high-resolution aMXD chronologies from this study are significantly positively correlated (p < 0.01) and are very similar to the original MXD chronology (Linderholm & Gunnarson, 2019), except in 1783 and 1784. The very high-resolution aMXD chronologies (aMXD10–aMXD40) have a 1783 value that is actually lower than 1784, while at lower measurement resolutions (aMXD50–aMXD160), 1783 has a higher aMXD value than 1784 (Figures 4b and 4c) and is in better agreement with the existing traditional MXD time series (Linderholm & Gunnarson, 2019). Irrespective of resolution, all of the aMXD chronologies are significantly and positively correlated with the CSCAN2019 MXD chronology; the correlation coefficient increases from the higher-resolution aMXD (aMXD20 m, r = 0.74) to lower-resolution aMXD (aMXD160, r = 0.92; Figure 5).

Examination of the wood anatomy in 1783 reveals the cause of these differences: an IADF in the later half of the ring, associated with a band of latewood cells with larger than average lumina that is followed by anomalously thin cell walls during the last part of growth (Figure 3). For the late 18th century, the automated IADF detection method identifies a slightly greater number of total IADFs overall compared to the simple visual identification

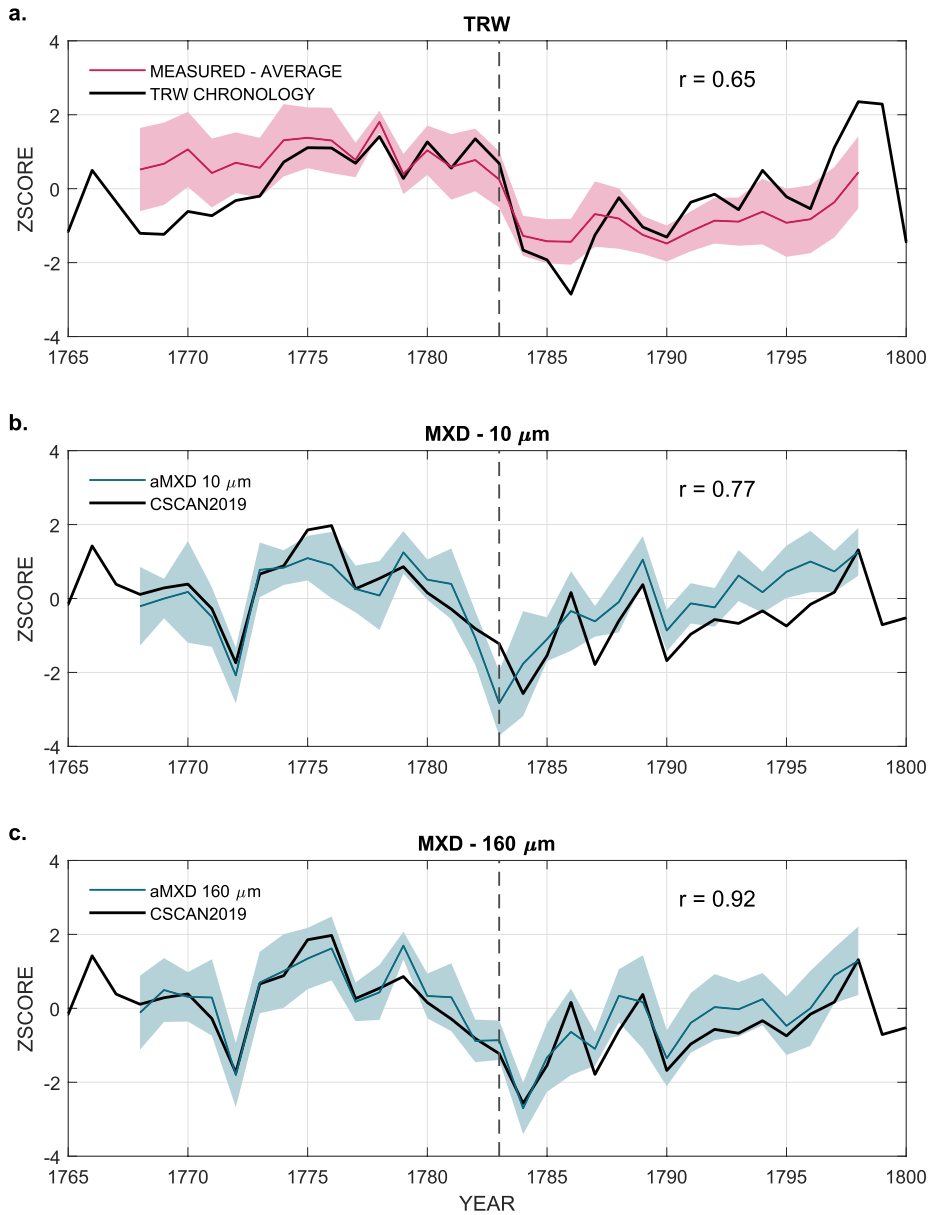

Figure 4. (a) Full sample ($N = 24$) tree-ring width (TRW) chronology (black line) and average tree-ring width of samples measured in ROXAS ($N = 9$, red line). (b), (c) Updated CSCAN2019 MXD chronology (black line) from Linderholm and Gunnarson (2019) and the anatomical MXD (aMXD) measurements (blue line) at a resolution of 10 μ (b) and 160 μ (c). Results from the Pearson correlation coefficient calculations are included in each plot. Values are normalized for comparison of the related, but different, measurements. The data in this study were analyzed over the 30-year period: 1768–1798. Shaded regions show the ±1 SD around the mean values. None of the anatomical chronologies were detrended. The aMXD10 has a lower correlation with the CSCAN2019 MXD chronology because of the drop in density in the last part of the ring that is captured by the high-resolution aMXD.

method (Figure 6). Using either method, however, 1783 has the highest occurrence of IADFs in the 1768–1798 period. With automatic detection, 1783 has IADFs in five out of nine cores. With visual identification, 1783 has IADFs in six out of nine cores. For non-Laki years, the largest number of cores with an IADF detected were two (visual) or three (automated). One sample (Fb06_20days) had very narrow rings and therefore no IADFs could be observed with the visual detection method.

Intraannual profiles of lumen area and cell wall area—the individual components that make up the anatomical density—reveal the cellular-level drivers of the IADFs in 1783 (Figure 7). While the 1783 Laki lumen area is

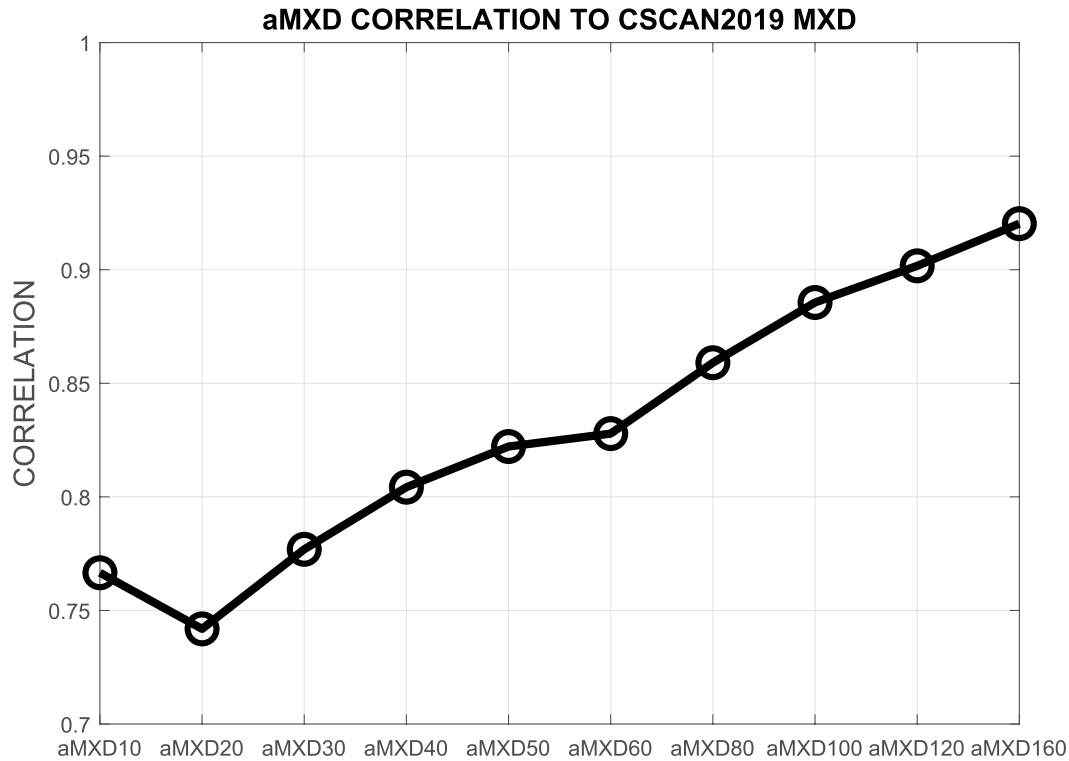

Figure 5. Results from the Pearson correlation coefficient calculations between the CSCAN2019 MXD chronology and each aMXD chronology from 1768 to 1798. All correlations are significant at $p < 0.001$.

actually larger than in noneruption control years for the first 50% of the total ring width, at between 60% and 80% of the total ring width the lumen area drops suddenly below the control (Figure 7a), indicating a premature end to the enlarging phase of xylogenesis for these cells. This rapid reduction is accompanied by a simultaneous decline in the cell wall area (Figure 7b), further indicating that cambial activity became suddenly disrupted at this time. While the Laki year lumen area plateaued and rose slightly above the control year median for the last 15% of the total ring width, the Laki cell wall area does not make a similar recovery and remains below the noneruption year median. The briefly higher density wood in the Laki year at 65%–80% of the total ring width (Figure 7c) is therefore associated with the abrupt decline in lumen area that defines the start of the IADF. For the remainder

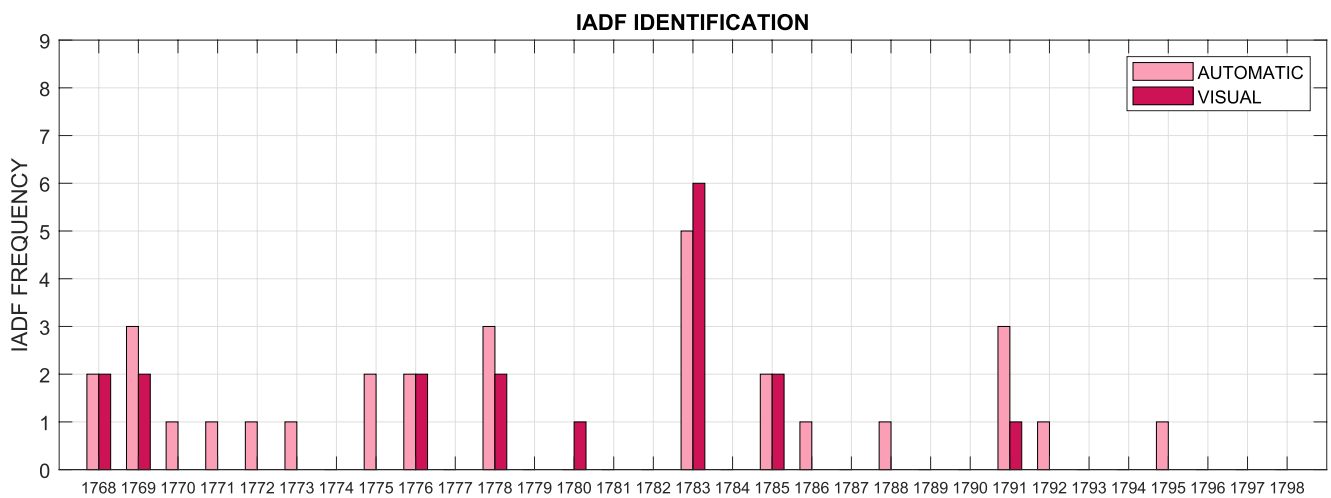

Figure 6. Intraannual density fluctuation (IADF) frequency from 1768 to 1798 CE based on automatic detection (light pink) and visual identification (dark park). Frequency is out of nine possible trees for every year for both identification methods.

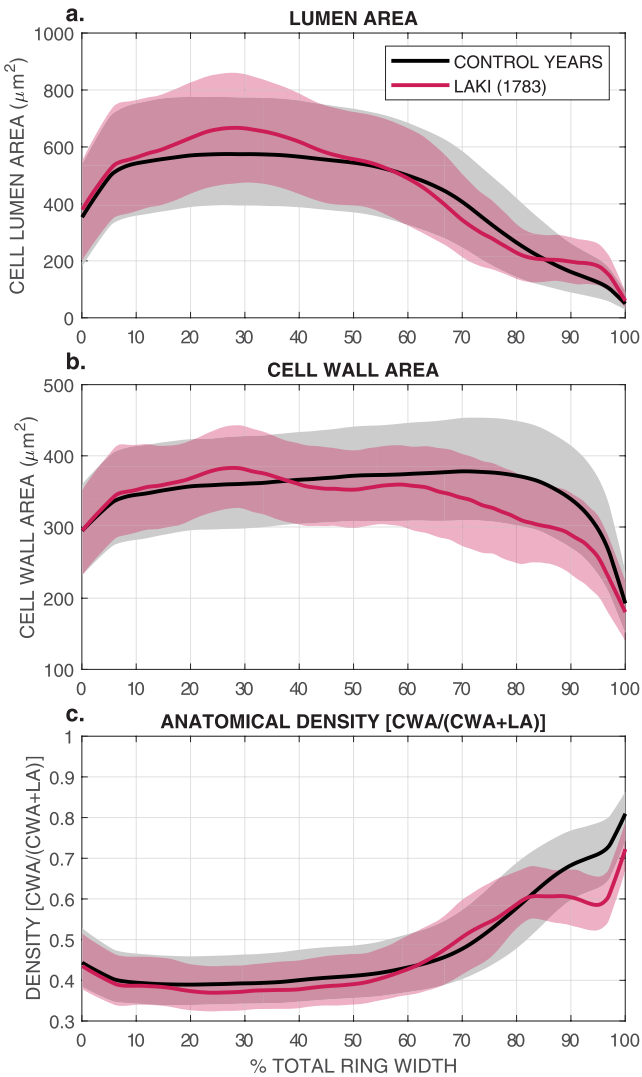

Figure 7. Lumen area, cell wall area, and anatomical density measurements plotted according to their relative position in the tree ring. The anatomical density is the ratio between the cell wall area (CWA) and the sum of cell wall area (CWA) and cell lumen area (LA). The red line is the lowess curve of all cell measurement for the 1783 years throughout the different relative positions in the ring. The red envelope represents the area between the lowess curves fit to the residuals of the original lowess curve. The black line is the lowess curve fit to all cell measurements of the control years: 15 years before and after the 1783 Laki eruption. The gray envelope represents the area between the lowess curves fit to the residuals of the original lowess curve for the control years.

of the growing season, the declining cell wall area combined with the plateau in lumen area resulted in the low density measured in the last 15% of the 1783 ring.

3.2. Climate Data

For the 1768–1798 period during the latter half of the Little Ice Age, the Stockholm, Uppsala, and Trondheim stations experienced cool summers with temperatures rising above 0°C by April (Figure 8). Temperatures for 1783 were higher than the 1768–1798 average, with notably higher temperatures particularly in April, July, and September at the Trondheim stations (Figure 8b). Temperatures in 1784 were consistently lower than the 1768–1798 average particularly in the winter of that year at both stations (Figures 8a and 8b). Daily data also show that Stockholm temperatures in the summer of 1783 were generally higher than the 1768–1798 average, except for a brief period in the beginning of August when temperature was on average 2.48°C below normal over a period of 5 days (Figure 8c). A comparison of modern weather observations from Östersund and Höglekardalen suggests the Jämtland tree-ring site is 0–2.5°C cooler than Trondheim and 3–5°C cooler than Uppsala.

All of the aMXD chronologies and CSCAN2019 are significantly and positively correlated with August temperature at both historical stations over the full 1768–1798 period (Figure 9). The highest correlation ($r = 0.65$) is between CSCAN2019 and August temperature at Uppsala, and the strongest aMXD correlation ($r = 0.60$) is between aMXD80 and August temperature at Uppsala. Both CSCAN2019 and the lower resolution aMXD (aMXD80–aMXD160) series have a broader seasonal range of months with significant correlations at the Uppsala station, although interestingly not at Trondheim (Figure 9a). The correlations with historical climate data from the 18th century are stronger overall if 1783 is excluded (not shown).

3.3. Carbon Isotope Data

The $\Delta^{13}C$ series has a large negative excursion at 1783–1785, with the largest decrease in isotopic discrimination in 1784 (Figure 10). If we consider the entirety of the 1768–1798 period, there is no significant correlation between any of the MXD chronologies and the $\Delta^{13}C$ series (Table 1). However, when we simply exclude 1783, 1784, and 1785 from the calculation, the expected (Gagen et al., 2007; Seftigen et al., 2011) significant negative correlation between the MXD chronologies and $\Delta^{13}C$ emerges. The absolute value of the correlation coefficient generally increases from high-resolution aMXD to low-resolution aMXD (Table 1), with the weakest negative correlation at aMXD20 ($r = -0.35$, $p = 0.07$), and the strongest negative correlation at aMXD160 ($r = -0.62$, $p < 0.01$). All correlations with 1783, 1784, and 1785 excluded are significant at $p \leq 0.07$ (Table 1).

3.4. X-Ray Fluorescence

Both sulfur and chlorine were below detection limits for our XRF analysis of these samples. Elements such as As, Br, Cu, and Zn—which could reflect an acidification response—do show a slight decrease in the latewood of the 1783 and 1784 rings, but this could also result from lower latewood density in these rings (Pearson et al., 2009). Similarly, Pearson et al. (2006) were not able to detect chemical evidence for the direct impact of eruption products from the Icelandic volcano Askja (1875) on trees growing downwind in central Sweden, although the Askja eruption also differed from the Laki eruption in many important respects. Dendrochemical studies generally

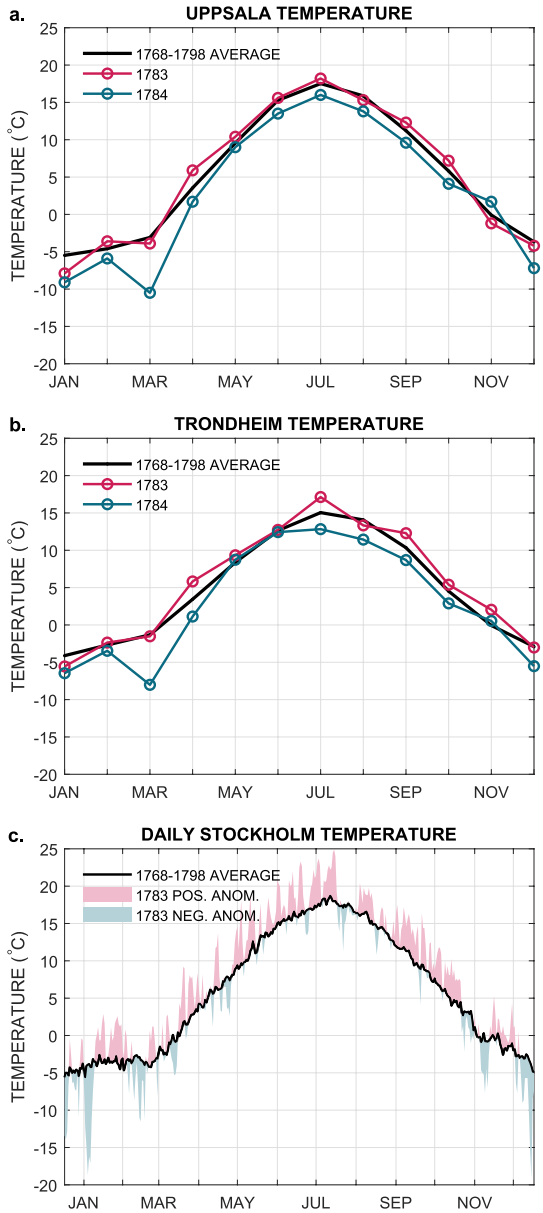

Figure 8. Historical monthly temperature data from the Uppsala (a) and the average Trondheim (b) climate stations. Temperature for 1783 CE (red), 1784 CE (blue), and the average temperature over the 1768–1798 CE period (black) are plotted (a, b). Daily temperature data from the Stockholm climate station (c): positive 1783 CE temperature anomalies over the 1768–1798 CE average (black) are plotted with red, while negative 1783 CE temperature anomalies are plotted with blue. *X*-axis tick marks in panel c mark the halfway point of each month.

show a high level of variability in-terms of tracing the onset of chemical change in the environment. Even for forests subject to relatively high levels of anthropogenically or volcanically produced pollutants, dendrochemical analyses have shown mixed results (Rocha et al., 2020; Watmough, 1997; Watt et al., 2007), due to a complex interplay of factors related to the size, spread, season, and proximity of the pollution event as well as to tree and micro-site specific variables (soil depth and chemistry, topography, etc). Even when eruptions do leave a geochemical trace in annual rings, individual trees may record different signals (Sheppard et al., 2009). Our dendrochemistry results, while compatible with an acid deposition hypothesis, were inconclusive, and cannot be strongly argued to support the direct impact of the acidic Laki haze on wood anatomical anomalies in 1783.

4. Discussion

4.1. Measurement Resolution, Extreme Events, and the Disruption of Wood Formation

Calculating aMXD using multiple different resolutions permits us to identify the complicated and abnormal intraannual tree-ring response to the Laki volcanic eruption (Figure 4), which in turn allows us to better understand the discrepancy between historical observations and traditional MXD (Figure 1). The MXD data from Jämtland used in the Luterbacher et al. (2016) reconstruction and others (e.g., Anchukaitis et al., 2017) were measured using the Itrax wood scanner (Gunnarson et al., 2011; Linderholm & Gunnarson, 2019). While the measurements were taken at nominal 20 μm steps (Linderholm & Gunnarson, 2019), Björklund et al. (2019) calculated an effective or apparent resolution for Itrax between 100 and 120 μm. The 10 μm resolution aMXD typically calculates the density in very last section of the latewood, which is relatively low in 1783 CE, as seen in Figure 3. The low MXD measured by the Itrax or the low resolution aMXD in 1783 is caused by the inclusion of this low density section in the very last portion of the latewood but then is ameliorated in part by incorporating the higher density portion of the IADF (Figure 4). In other words, the lower effective resolution of the Itrax data coincidentally compensates somewhat for the very low wood density detected by our highest resolution aMXD calculations. Our use of the high-resolution aMXD measurements shows that IADFs in 1783 are caused by disruptions to the normal anatomical structure of the annual ring. When the normal wood formation is disturbed, as it is here after the eruption, the expected relationship between summer temperature and traditional MXD measurements appears to be altered.

4.2. Potential Causes of Low MXD and IADFs in 1783

IADFs are the result of deviations from the normal growing season patterns of xylogenesis (De Micco et al., 2016; Mayer et al., 2020). The characteristic density fluctuations of IADFs can form due to changes in cell differentiation or bimodal cambial activity: in our case, cambial activity declines and smaller abnormal cells are produced due to detrimental growing conditions (Battipaglia et al., 2016; De Micco et al., 2016; Morino et al., 2021; Wimmer et al., 2000). Anatomical anomalies like IADFs are generally formed when trees experience stressful conditions, including drought, defoliation, or frost events (Cuny et al., 2014; Fritts, 1976). IADFs have been commonly linked to changes in moisture availability in trees from Mediterranean or bimodal precipitation monsoon regions (Morino et al., 2021), but are rarely found in boreal forest trees and have only been observed in ≈9% of tree rings in previous studies (Battipaglia et al., 2016). However, in boreal

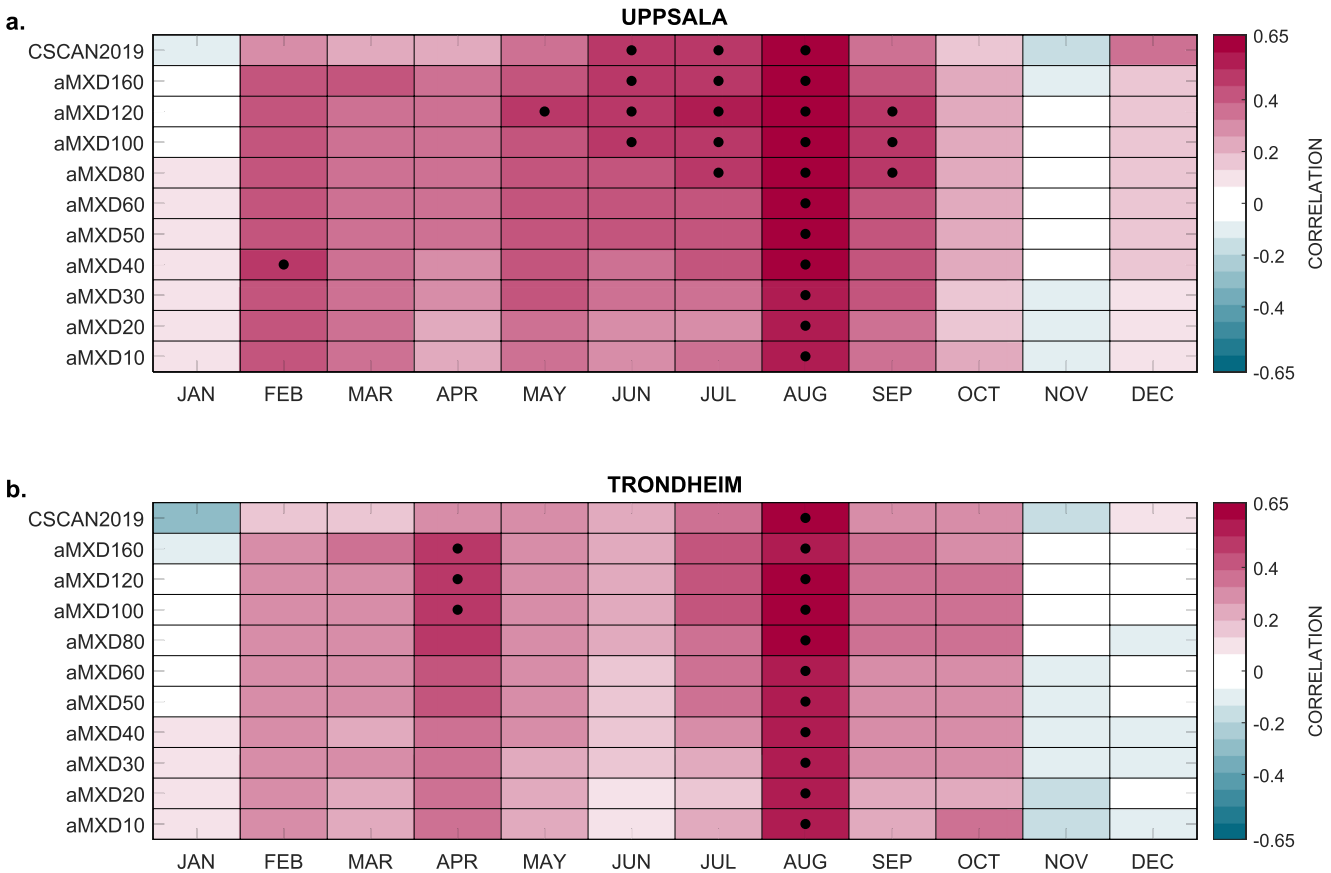

Figure 9. Results from the Pearson correlation coefficient calculations between the monthly data at Uppsala (a) and Trondheim (b), and the multiple resolution aMXD and CSCAN2019 MXD chronologies from 1768 to 1798 CE. Significant correlations ($\alpha = 0.01$) are indicated with a dot.

forests the occurrence of IADFs can be the result of defoliation from pollution or sudden cold events (Kozlov & Kisternaya, 2004; Kurczyńska et al., 1997) and IADFs are more commonly observed in wider rings (Battipaglia et al., 2016; De Micco et al., 2016). The IADFs we observe in 1783 originate from an initial sharp decline in lumen area in the later section of the ring, concomitant with a decline in cell wall area in the latewood, which

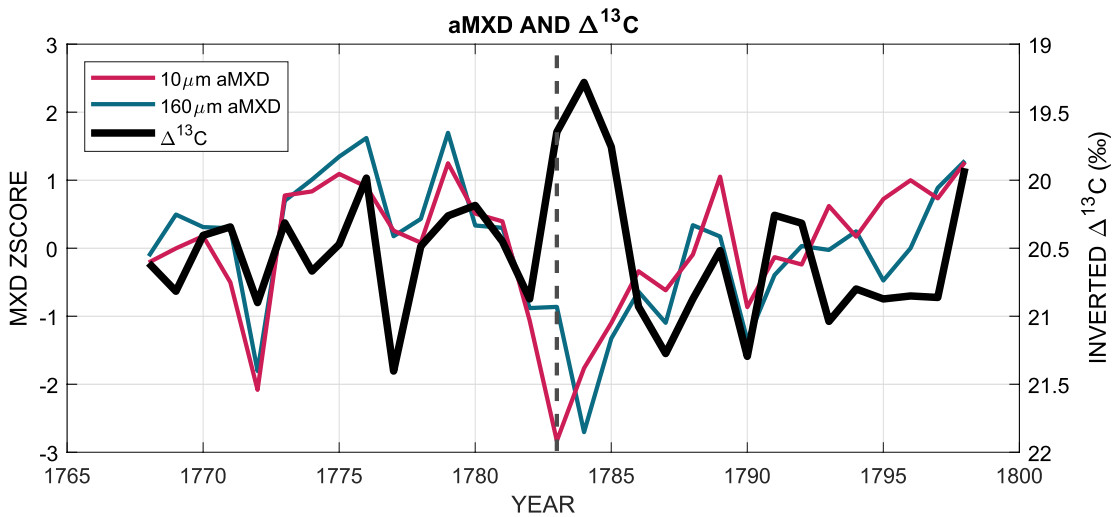

Figure 10. Times series of $\Delta^{13}C$ (black) converted from (Seftigen et al., 2011) and aMXD chronologies at the 10 μm resolution (red) and at the 160 μm resolution (blue). aMXD chronologies are normalized. The $\Delta^{13}C$ time series axis is inverted for better visual interpretation.

Table 1
Results From the Pearson Correlation Coefficient Calculations Between the $\Delta^{13}C$ Series (Seftigen et al., 2011) and the Multiple Resolution aMXD and CSCAN2019 MXD Chronologies From 1768 to 1798, With and Without Excluding Concurrent and Post-Volcanic Eruption Years 1783, 1784, and 1785

Chronology	1768–1798 *r*	1768–1798 *p*-value	1783–1785 excluded *r*	1783–1785 excluded *p*-values
aMXD10	0.18	0.32	−0.43	0.02
aMXD20	0.23	0.21	−0.35	0.07
aMXD30	0.22	0.23	−0.38	0.05
aMXD40	0.17	0.36	−0.44	0.02
aMXD50	0.17	0.37	−0.46	0.01
aMXD60	0.15	0.43	−0.48	<0.01
aMXD80	0.12	0.53	−0.52	<0.01
aMXD100	0.08	0.69	−0.56	<0.01
aMXD120	0.05	0.80	−0.59	<0.01
aMXD160	0.02	0.91	−0.62	<0.01
CSCAN2019	−0.03	0.88	−0.60	<0.01

results in a temporary increase in anatomical density followed by a reduction at the very end of the year, relative to the control years (Figure 7).

Based on multiple lines of evidence discussed in detail below, we hypothesize that the high prevalence of IADFs in 1783 was most likely caused by acid damage from the volcanic eruption and is linked to the anomalous MXD values in that year. Our assessment rules out temperature changes through comparison between the multiple MXD chronologies, historical observations, and the $\Delta^{13}C$ record. We cannot, however, conclusively parse the possible effect of changes to light availability as the Furuberget $\Delta^{13}C$ chronology appears to be overwhelmed by the direct effect of the acidic haze.

We interpret the low MXD and high frequency of IADFs in 1783 to most likely be a consequence of the direct and detrimental effect of the Laki eruption's acidic haze on tree growth, as hypothesized by Briffa et al. (1988). Historical observations in both Sweden and Norway at the time noted acidic haze and concurrent vegetation damage (Demarée & Ogilvie, 2001; Grattan & Pyatt, 1994; Laufeld, 1994; Thorarinsson, 1981). The grain harvest also failed in several parts of Sweden in September 1783 and the hay harvest produced low yields (Demarée & Ogilvie, 2001). In Trondheim, tree leaves were described as "burnt" and vegetation "withered" after acid rain and fog deposition respectively (Demarée & Ogilvie, 2001). In Sweden, the dry fog was observed to be "injurious to the vegetation" and that it "damaged the trees" and caused plants to "wither and drop their leaves" (Thorarinsson, 1981). Reports in western Europe similarly describe trees losing their leaves suddenly, and vegetation looking "burnt" or that it had the "appearances of the autumn" (Demarée & Ogilvie, 2001). Volcanic pollutants including SO_2 and H_2S are known to damage conifer needles, which leads to a reduction of stomatal aperture and potentially defoliation and even tree death (Bartiromo et al., 2012). SO_2 and SO_4-induced damage to needle stomata also limits photosynthetic CO_2 fixation and causes preferential uptake of ^{13}C (D'Arcy et al., 2019; Martin et al., 1988; Thomas et al., 2013), which is consistent with the decrease in carbon isotope discrimination we observe in the Furuberget $\Delta^{13}C$. Trees under consistent industrial sulfur pollution have also displayed reduced MXD and increased occurrences of IADFs compared to trees at nonpolluted sites (Kurczyńska et al., 1997; Wimmer, 2002). A study by Myśkow et al. (2019) demonstrated that pollutant fog deposition resulted in decreased cambial activity, leading to the formation of narrower annual rings such as those observed at Jämtland in the years following the eruption (Figure 4). Ring-width suppression and needle damage in *P. sylvestris* has similarly been reported in association with artificial smoke, containing chlorosulfonic acid, used to conceal the location of the German battleships Tirpitz during the Second World War (Hartl et al., 2019) and as the result of insect induced defoliation (Axelson et al., 2014; Watanabe & Ohno, 2020). A number of investigators have found additionally that latewood width, latewood density, and cell wall thickness can all be reduced by defoliation (Arbellay et al., 2018; Castagneri et al., 2020; Esper et al., 2007).

A combination of the atmospheric conditions at the time of the Laki eruption and, potentially the influence of site topography, likely led to long-lasting and effective volcanic pollutant deposition at our study site. Volcanic gas concentration and persistence have a direct effect on the severity of damage to vegetation (Bartiromo et al., 2012; Delmelle, 2003). Acidified fog can potentially have 10 times the solute concentration compared to rain, and has greater capacity for vegetation damage (Delmelle, 2003). The high pressure cell and atmospheric blocking over Europe at the time of the Laki eruption also led to a more persistent sulfuric surface haze (Thordarson & Self, 2003; Zambri et al., 2019a). Modeling experiments show high surface sulfate aerosol concentrations over central Sweden throughout the summer (Chenet et al., 2005) and historical observations from Stockholm first note a "dry fog" on 24 June, which then continued every day for a month, except for 4 days at the end of June/early July (Thorarinsson, 1981; Thordarson & Self, 2003). Model simulations of the Laki eruption show peak sulfate loading in the upper troposphere/lower stratosphere in August (Oman et al., 2006; Zambri et al., 2019b), the time period when temperature would otherwise normally be the primary influence on MXD (Figure 9). The timing of the eruption is crucial because it occurred during the boreal forest growing season. While defoliation effects can lead to subsequent growth suppression irrespective of season, the sudden change in xylogenesis we observe

imprinted on the wood anatomy of 1783 is likely the result of the acidic haze and tree damage during a period of active cambial growth. Previous studies have also found a positive relationship between elevation and sulfate deposition, with fogwater deposition more significant than deposition from precipitation at higher elevations (Lükewille & Semb, 1997; Walmsley et al., 1970). While the trees in the full data set were collectively sampled over a wide area, the majority of the trees used here for QWA analysis were sampled on the top of a small peak at approximately 650 m a.s.l (Linderholm & Gunnarson, 2019), possibly making them even more susceptible to the direct effects of the haze (Delmelle, 2003).

In theory, a sudden or transient cold period could also cause low density in the very last section of the 1783 ring (cf. Edwards et al., 2021; Piermattei et al., 2020). At lower measurement resolution both traditional MXD and aMXD chronologies reflect temperatures integrated over the entire summer, while the high-resolution aMXD chronologies capture the anatomical characteristics of only late growing season August temperature (Figure 9). The higher resolution aMXD chronologies (Figure 4b) are therefore capable of capturing a monthly or even sub-monthly climate signal caused by a brief cold period at the end of the growing season, as occurred in Alaska following the Laki eruption (Edwards et al., 2021). The monthly data from the Uppsala and Trondheim stations may be too coarse, however, to properly identify such a period. Daily data from Stockholm does show a 5-day period of cooler temperature anomalies (−2.48°C below climatology over the 5-day period) in the beginning of August (Figure 8c). However, this period is unlikely to be long enough nor sufficiently severe to cause the anomalous wood anatomy and low MXD seen in the 1783 ring (Begum et al., 2012). Low August and September temperatures that cause an early end to the growing season, as well as ephemeral cold snaps, have been previously linked to lower MXD and associated with "light rings" (Edwards et al., 2021; Gindl et al., 2000; Szeicz, 1996; Vaganov et al., 2006) or "blue rings" (Björklund et al., 2021; Matisons et al., 2020; Piermattei et al., 2015; Piermattei et al., 2020), neither of which are observed in the 1783 rings. Damage to vegetation from Laki acid deposition was often at the time erroneously attributed to overnight frost in England and across Europe, including in Sweden (Grattan & Pyatt, 1994; Thordarson & Self, 2003). But because early morning and evening temperatures were recorded to be well above freezing (10–15°C), it is unlikely that temperatures would drop below freezing in the few hours between measurements (Thordarson & Self, 2003). There is a negative temperature anomaly at the beginning of May in Stockholm (Figure 8c) and mild frosts in late spring/early summer have been previously linked to IADF occurrence (Kozlov & Kisternaya, 2004). However, early season climate conditions are more commonly associated with IADFs defined by latewood-like cells within the earlywood, rather than the type of IADFs we see in 1783, which is defined by earlywood-like cells within the latewood (Campelo et al., 2007; De Micco et al., 2016).

An alternative hypothesis is that the low MXD in 1783 could be caused by a decrease in light availability after the Laki eruption, overwhelming the proxy's normal temperature response. For instance, Tingley et al. (2014) suggest that low MXD in years following volcanic eruptions could be caused by light reduction. In contrast, the Furuberget $\Delta^{13}C$ record (Figure 10) would conventionally be interpreted as indicating an *increase* in light availability during and after the Laki eruption (Figure 10), as tree-ring $\delta^{13}C$ records from this region have been shown to positively covary with sunshine metrics (Gagen et al., 2007; Loader et al., 2013; Seftigen et al., 2011). The negative $\Delta^{13}C$ excursion may be because an increase in diffuse radiation caused by light scattering from volcanic aerosols (Robock, 2005) actually increased photosynthetic capacity. Diffuse radiation has been hypothesized to lead to more efficient photosynthesis (Gu et al., 2003; Mercado et al., 2009) and so if anything would presumably result in an increase in MXD (Robock, 2005). There are, however, contrasting findings in this regard (e.g., Knohl & Baldocchi, 2008). Furthermore, there is no evidence from either TRW or MXD that growth conditions during the summer of 1783 were more favorable due to increased diffuse light. The negative $\Delta^{13}C$ excursion observed in 1783 is, however, the expected response to a decrease in carbon isotope discrimination caused by historically supported acid deposition (Rayback et al., 2020). Other tree-ring $\delta^{13}C$ records from further north in Fennoscandia, however, are unremarkable in 1783 and do not indicate any consistent changes in cloud cover or light availability over the broader region (Loader et al., 2013; Young et al., 2012). Thus, while we cannot eliminate a potential role for changing light availability during the eruption in 1783, the carbon isotope evidence from Furuberget is most consistent with the expected response to direct damage to trees from acidic haze. Beyond tree-ring data, analysis of historical documents may in the future be able to provide additional information on changes in light or diffuse radiation caused by the Laki eruption.

Lumen area is also normally correlated with day length over the course of the growing season, with the longer photoperiod of summer promoting the production of auxin, the phytohormone responsible for cell growth and extensibility (Buttò et al., 2021; Cuny et al., 2014; Cuny & Rathgeber, 2016; Rathgeber et al., 2016). Oman et al. (2006) simulated a strong decrease in surface shortwave radiation during the summer 1783 and contemporary accounts report the "sky was overspread with a dark dry fog" (Brayshay & Grattan, 1999). However, it is not clear what the response of the cambium might be to a *sudden* change in photosynthetically available radiation during the eruption or how this would be reflected in the lumen anatomy for that year. Experimental and observational evidence of the cambial response to sudden changes in light following volcanic eruptions may help further parse the relative contributions to the haze itself and the concomitant alteration of surface radiation.

4.3. Abnormal Wood Anatomy Disrupts MXD Temperature Signals

While one would expect to observe high MXD values in 1783 given the high temperatures recorded across Scandinavia (Figure 8), the direct effects of the volcanic haze appear to be the best explanation for the disrupted climate signal. In the first 50% of the total ring width, the 1783 lumen area is higher than the control period average, as might be expected during a warm spring and the generally favorable growing conditions seen in historical records, but it then sharply declines at 60% through the annual ring (Figure 7a). This decrease in lumen area leads to a temporary increase in density, but reduced cell wall area ultimately leads to low density in the last 15% of the total ring width and the low MXD value in 1783 (Figure 7). Vejpustková et al. (2017) found that lumen width, cell wall thickness, and cell number all decreased following an industrial SO_2 pollution event and Myśkow et al. (2019) found that earlywood cell width and lumen area decreased during intense pollutant deposition. Other studies have also shown that industrial sulfur pollution leads to reduced MXD and increased occurrence of IADFs compared to trees at nonpolluted sites (Evertsen et al., 1986; Kurczyńska et al., 1997; Wimmer, 2002). In 1783, the cell wall area in the Jämtland trees decreases below the noneruption year average at the same time as the lumen area declines but never recovers, which ultimately leads to the low MXD for the year (Figure 7b). Normally, we expect cell wall area to remain approximately fixed throughout the ring except for the very last cells that respond to climate conditions (Cuny et al., 2014), so the decrease in cell wall area and the other anatomical anomalies that we observe in 1783 indicates a disturbance of the normal wood formation process.

The wood anatomical anomalies we observe in 1783 should be considered exceptional, because events like the Laki eruption are relatively rare (Toohey et al., 2019) and its direct effects were exacerbated by atmospheric circulation patterns at the time (Zambri et al., 2019a). More generally, the proximal impacts of large eruptions on tree-ring formation will be limited geographically, and at hemispheric and global scales the climate signal of eruptions should still dominate in temperature-sensitive tree-ring chronologies. However, it is possible that other eruptions may have had similar effects. For instance, while the exact source of the extratropical volcanic eruption in 536 CE remains unknown (Helama et al., 2018; Sigl et al., 2015; Stothers & Rampino, 1983), records from across the Mediterranean (Stothers & Rampino, 1983) recall what would seem to be the impacts of an acid fog highly reminiscent of Laki period descriptions. Future work might focus on trees from regions where such records are prevalent and, where the source volcano is known, tested in any remaining forests in close proximity.

5. Conclusion

By using wood anatomical data in combination with stable carbon isotope data and historical observations, we identified the cause of the discrepancy between historical observations and traditional MXD chronologies following the 1783 Laki eruption. We found anomalous wood anatomy, a high prevalence of IADFs, and reduced lumen and cell wall area in the latewood of 1783, which we interpret to most likely be the consequence of damage to wood formation processes by volcanic acid deposition on wood formation processes. In contrast, 1784 shows the expected climatic response (cooling as a result of stratospheric sulfate)—lower MXD—in agreement with historical records. The decline in tree-ring width in 1784 and for several years afterward might also in part reflect the ongoing effects of the acid induced defoliation that occurred in 1783 (Axelson et al., 2014; Hartl et al., 2019).

The results of this study have implications for the interpretation of tree-ring records following proximal volcanic eruptions. In the case of tree rings formed during the Laki eruption, we clearly demonstrate that the normal climate/MXD relationship is disrupted or obfuscated by the anatomical consequences of what is most likely the direct effects of acidic haze. Under normal circumstance, the high-resolution density estimates made possible

by quantitative wood anatomy can provide very precise estimates of past temperature trends and variability (Björklund et al., 2020), but the ability to vary the effective resolution of these measurements also suggests a potential approach for identifying anomalous years associated with rare disturbances or extreme environmental events. However, it is not yet clear that it is possible to recover the "true" temperature signature from rings where anatomical anomalies reflect a nonclimatic cause. Further work is necessary to determine how best to use aMXD records to analyze and quantify these extreme years, but our study already suggests that screening anatomical series for anomalies can lead to an evaluation of potentially confounding factors for climate reconstructions. In the case of the Laki eruption specifically, wood anatomy allows us to understand why existing tree-ring reconstructions of summer temperature using MXD do not agree with historical records and observations. In addition to the previously established effects of the Laki eruption haze on human health, our study underlines the potential detrimental effect of acid volcanic haze on forest vegetation, underscoring the wide-ranging impact that such eruptions can have across a large region.

Data Availability Statement

The tree-ring data that support the findings of this study are available in the International Tree-Ring Data Bank (ITRDB) at the NOAA/World Data Service for Paleoclimatology archives (https://www.ncdc.noaa.gov/paleo/study/35258). The data on which this article is based are available in Luterbacher et al. (2004), Seftigen et al. (2011), Luterbacher et al. (2016), Linderholm and Gunnarson (2019); Moberg (2020), and the Berkeley Earth compilation (Lawrimore et al., 2011; Menne et al., 2018; Rohde & Hausfather, 2020).

Acknowledgments
Kevin J. Anchukaitis thanks Alan Robock, Brian Zambri, and the local organizers for discussions at the Past Global Changes (PAGES) "Volcanic Impacts on Climate and Society" (VICS) meeting in Cambridge about the reconstructed and historical climate discrepancy in Europe during the Laki eruption. The authors thank Talia Anderson for assisting with visual IADF identification and Soumaya Belmecheri for additional discussions about carbon isotopes. The authors also thank Katrin Kleemann and Alma Piermattei for comments and suggestions that substantially improved the manuscript. In particular, the uthors acknowledge Dr. Kleemann for directing us toward additional historical information that will be included in her forthcoming book, *A Mist Connection: An Environmental History of the Laki Eruption of 1783 and Its Legacy*. Julie Edwards and Kevin J. Anchukaitis were partially supported by NSF P2C2 grant AGS-2102993. Kristina Seftigen and Georg von Arx were supported by the Swiss National Science Foundation SNSF (grant no. 200021_182398, XELLCLIM).

References

Anchukaitis, K. J., Wilson, R., Briffa, K. R., Buntgen, U., Cook, E. R., D'Arrigo, R., et al. (2017). Last millennium northern hemisphere summer temperatures from tree rings: Part II, spatially resolved reconstructions. *Quaternary Science Reviews*, *163*, 1–22. https://doi.org/10.1016/j.quascirev.2017.02.020

Arbellay, E., Jarvis, I., Chavardès, R. D., Daniels, L. D., & Stoffel, M. (2018). Tree-ring proxies of larch bud moth defoliation: Latewood width and blue intensity are more precise than tree-ring width. *Tree Physiology*, *38*(8), 1237–1245. https://doi.org/10.1093/treephys/tpy057

Auker, M. R., Sparks, R. S. J., Siebert, L., Crosweller, H. S., & Ewert, J. (2013). A statistical analysis of the global historical volcanic fatalities record. *Journal of Applied Volcanology*, *2*(1). 1–24. https://doi.org/10.1186/2191-5040-2-2

Axelson, J., Bast, A., Alfaro, R., Smith, D., & Gärtner, H. (2014). Variation in wood anatomical structure of Douglas-fir defoliated by the western spruce budworm: A case study in the coastal-transitional zone of British Columbia, Canada. *Trees*, *28*(6), 1837–1846. https://doi.org/10.1007/s00468-014-1091-1

Bartiromo, A., Guignard, G., Lumaga, M. R. B., Barattolo, F., Chiodini, G., Avino, R., et al. (2012). Influence of volcanic gases on the epidermis of Pinus halepensis Mill. in Campi Flegrei, southern Italy: A possible tool for detecting volcanism in present and past floras. *Journal of Volcanology and Geothermal Research*, *233–234*, 1–17. https://doi.org/10.1016/j.jvolgeores.2012.04.002

Battipaglia, G., Campelo, F., Vieira, J., Grabner, M., De Micco, V., Nabais, C., et al. (2016). Structure and function of intra–annual density fluctuations: Mind the gaps. *Frontiers of Plant Science*, *7*, 595. https://doi.org/10.3389/fpls.2016.00595

Bauska, T. K., Joos, F., Mix, A. C., Roth, R., Ahn, J., & Brook, E. J. (2015). Links between atmospheric carbon dioxide, the land carbon reservoir and climate over the past millennium. *Nature Geoscience*, *8*(5), 383–387. https://doi.org/10.1038/ngeo2422

Begum, S., Nakaba, S., Islam, M. A., Yamagishi, Y., & Funada, R. (2012). Effects of low temperature in reactivated cambial cells induced by localized heating during winter dormancy in conifers. *American Journal of Plant Physiology*, *7*(1), 30–40. https://doi.org/10.3923/ajpp.2012.30.40

Belmecheri, S., & Lavergne, A. (2020). Compiled records of atmospheric CO_2 concentrations and stable carbon isotopes to reconstruct climate and derive plant ecophysiological indices from tree rings. *Dendrochronologia*, *63*(125), 748. https://doi.org/10.1016/j.dendro.2020.125748

Binda, G., Di Iorio, A., & Monticelli, D. (2021). The what, how, why, and when of dendrochemistry: (paleo) environmental information from the chemical analysis of tree rings. *The Science of the Total Environment*, *758*(143), 672. https://doi.org/10.1016/j.scitotenv.2020.143672

Björklund, J., Arx, G., Nievergelt, D., Wilson, R., den Bulcke, J. V., Günther, B., et al. (2019). Scientific merits and analytical challenges of tree-ring densitometry. *Reviews of Geophysics*, *57*(4), 1224–1264. https://doi.org/10.1029/2019rg000642

Björklund, J., Fonti, M. V., Fonti, P., Van den Bulcke, J., & von Arx, G. (2021). Cell wall dimensions reign supreme: Cell wall composition is irrelevant for the temperature signal of latewood density/blue intensity in Scots pine. *Dendrochronologia*, *65*(125), 785. https://doi.org/10.1016/j.dendro.2020.125785

Björklund, J., Seftigen, K., Fonti, P., Nievergelt, D., & von Arx, G. (2020). Dendroclimatic potential of dendroanatomy in temperature-sensitive Pinus sylvestris. *Dendrochronologia*, *60*, 125673. https://doi.org/10.1016/j.dendro.2020.125673

Brayshay, M., & Grattan, J. (1999). Environmental and social responses in Europe to the 1783 eruption of the Laki fissure volcano in Iceland: A consideration of contemporary documentary evidence. *Geological Society, London, Special Publications*, *161*(1), 173–187. https://doi.org/10.1144/gsl.sp.1999.161.01.12

Briffa, K. R., Jones, P. D., Pilcher, J. R., & Hughes, M. K. (1988). Reconstructing summer temperatures in northern Fennoscandinavia back to A.D. 1700 using tree-ring data from Scots pine. *Arctic and Alpine Research*, *20*(4), 385–394. https://doi.org/10.2307/1551336

Brown, S. K., Auker, M., & Sparks, R. (2015). Populations around Holocene volcanoes and development of a population exposure index. In *Global volcanic hazards and risk* (pp. 223–232). Cambridge University Press. https://doi.org/10.1017/cbo9781316276273.006

Budd, L., Griggs, S., Howarth, D., & Ison, S. (2011). A fiasco of volcanic proportions? Eyjafjallajökull and the closure of European airspace. *Mobilities*, *6*(1), 31–40. https://doi.org/10.1080/17450101.2011.532650

Bunn, A. G. (2008). A dendrochronology program library in R (dplR). *Dendrochronologia*, *26*(2), 115–124. https://doi.org/10.1016/j.dendro.2008.01.002

Buttò, V., Rozenberg, P., Deslauriers, A., Rossi, S., & Morin, H. (2021). Environmental and developmental factors driving xylem anatomy and micro-density in black spruce. *New Phytologist*, *230*(3), 957–971. https://doi.org/10.1111/nph.17223
Campelo, F., Nabais, C., Freitas, H., & Gutiérrez, E. (2007). Climatic significance of tree-ring width and intra-annual density fluctuations in Pinus pinea from a dry Mediterranean area in Portugal. *Annals of Forest Science*, *64*(2), 229–238. https://doi.org/10.1051/forest:2006107
Carlsen, H. K., Hauksdottir, A., Valdimarsdottir, U. A., Gíslason, T., Einarsdottir, G., Runolfsson, H., et al. (2012). Health effects following the Eyjafjallajökull volcanic eruption: A cohort study. *BMJ Open*, *2*(6), e001851. https://doi.org/10.1136/bmjopen-2012-001851
Carlsen, H. K., Ilyinskaya, E., Baxter, P. J., Schmidt, A., Thorsteinsson, T., Pfeffer, M. A., et al. (2021). Increased respiratory morbidity associated with exposure to a mature volcanic plume from a large Icelandic fissure eruption. *Nature Communications*, *12*(1), 1–12. https://doi.org/10.1038/s41467-021-22432-5
Carrer, M., Unterholzner, L., & Castagneri, D. (2018). Wood anatomical traits highlight complex temperature influence on Pinus cembra at high elevation in the Eastern Alps. *International Journal of Biometeorology*, *62*(9), 1745–1753. https://doi.org/10.1007/s00484-018-1577-4
Castagneri, D., Prendin, A. L., Peters, R. L., Carrer, M., von Arx, G., & Fonti, P. (2020). Long-term impacts of defoliator outbreaks on larch xylem structure and tree-ring biomass. *Frontiers of Plant Science*, *11*, 1078. https://doi.org/10.3389/fpls.2020.01078
Chenet, A.-L., Fluteau, F., & Courtillot, V. (2005). Modelling massive sulphate aerosol pollution, following the large 1783 Laki basaltic eruption. *Earth and Planetary Science Letters*, *236*(3–4), 721–731. https://doi.org/10.1016/j.epsl.2005.04.046
Cleveland, W. S. (1979). Robust locally weighted regression and smoothing scatterplots. *Journal of the American Statistical Association*, *74*(368), 829–836. https://doi.org/10.1080/01621459.1979.10481038
Cuny, H. E., & Rathgeber, C. B. (2016). Xylogenesis: Coniferous trees of temperate forests are listening to the climate tale during the growing season but only remember the last words. *Plant Physiology*, *171*(1), 306–317. https://doi.org/10.1104/pp.16.00037
Cuny, H. E., Rathgeber, C. B. K., Frank, D., Fonti, P., & Fournier, M. (2014). Kinetics of tracheid development explain conifer tree-ring structure. *New Phytologist*, *203*(4), 1231–1241. https://doi.org/10.1111/nph.12871
Damby, D. E., Horwell, C. J., Larsen, G., Thordarson, T., Tomatis, M., Fubini, B., & Donaldson, K. (2017). Assessment of the potential respiratory hazard of volcanic ash from future Icelandic eruptions: A study of archived basaltic to rhyolitic ash samples. *Environmental Health*, *16*(1), 1–15. https://doi.org/10.1186/s12940-017-0302-9
D'Arcy, F., Boucher, É., De Moor, J. M., Hélie, J.-F., Piggott, R., & Stix, J. (2019). Carbon and sulfur isotopes in tree rings as a proxy for volcanic degassing. *Geology*, *47*(9), 825–828.
D'Arrigo, R., Seager, R., Smerdon, J. E., LeGrande, A. N., & Cook, E. R. (2011). The anomalous winter of 1783-1784: Was the Laki eruption or an analog of the 2009-2010 winter to blame? *Geophysical Research Letters*, *38*(5). https://doi.org/10.1029/2011gl046696
D'Arrigo, R., Wilson, R., & Anchukaitis, K. J. (2013). Volcanic cooling signal in tree ring temperature records for the past millennium. *Journal of Geophysical Research: Atmospheres*, *118*(16), 9000–9010. https://doi.org/10.1002/jgrd.50692
Dawson, A. G., Kirkbride, M. P., & Cole, H. (2021). Atmospheric effects in Scotland of the AD 1783–84 Laki eruption in Iceland. *The Holocene*, *31*(5), 830–843. https://doi.org/10.1177/0959683620988052
De Micco, V., Campelo, F., De Luis, M., Bräuning, A., Grabner, M., Battipaglia, G., & Cherubini, P. (2016). Intra-annual density fluctuations in tree rings: How, when, where, and why? *IAWA Journal*, *37*(2), 232–259. https://doi.org/10.1163/22941932-20160132
Delmelle, P. (2003). Environmental impacts of tropospheric volcanic gas plumes. *Geological Society, London, Special Publications*, *213*(1), 381–399. https://doi.org/10.1144/gsl.sp.2003.213.01.23
Demarée, G. R., & Ogilvie, A. E. (2001). Bons Baisers d'Islande: Climatic, environmental, and human dimensions impacts of the Lakagígar eruption (1783–1784) in Iceland. In *History and climate* (pp. 219–246). Springer. https://doi.org/10.1007/978-1-4757-3365-5_11
Durand, M., & Grattan, J. (1999). Extensive respiratory health effects of volcanogenic dry fog in 1783 inferred from European documentary sources. *Environmental Geochemistry and Health*, *21*(4), 371–376. https://doi.org/10.1023/a:1006700921208
Edwards, J., Anchukaitis, K. J., Zambri, B., Andreu-Hayles, L., Oelkers, R., D'Arrigo, R., & von Arx, G. (2021). Intra-annual climate anomalies in Northwestern North America following the 1783–1784 CE Laki eruption. *Journal of Geophysical Research: Atmospheres*, *126*(3), e2020JD03544. https://doi.org/10.1029/2020JD033544
Eggleston, S., Schmitt, J., Bereiter, B., Schneider, R., & Fischer, H. (2016). Evolution of the stable carbon isotope composition of atmospheric CO_2 over the last glacial cycle. *Paleoceanography*, *31*(3), 434–452. https://doi.org/10.1002/2015pa002874
Esper, J., Büntgen, U., Frank, D. C., Nievergelt, D., & Liebhold, A. (2007). 1200 years of regular outbreaks in alpine insects. *Proceedings of the Royal Society B: Biological Sciences*, *274*(1610), 671–679. https://doi.org/10.1098/rspb.2006.0191
Esper, J., George, S. S., Anchukaitis, K., D'Arrigo, R., Ljungqvist, F. C., Luterbacher, J., et al. (2018). Large-scale, millennial-length temperature reconstructions from tree-rings. *Dendrochronologia*, *50*, 81–90. https://doi.org/10.1016/j.dendro.2018.06.001
Esper, J., Schneider, L., Smerdon, J. E., Schöne, B. R., & Büntgen, U. (2015). Signals and memory in tree-ring width and density data. *Dendrochronologia*, *35*, 62–70. https://doi.org/10.1016/j.dendro.2015.07.001
Evertsen, J., Mac Siurtain, M., & Gardiner, J. (1986). The effect of industrial emission on wood quality in Norway spruce (*Picea abies*). *IAWA Journal*, *7*(4), 399–404. https://doi.org/10.1163/22941932-90001010
Fairchild, I. J., Loader, N. J., Wynn, P. M., Frisia, S., Thomas, P. A., Lageard, J. G., et al. (2009). Sulfur fixation in wood mapped by synchrotron X-ray studies: Implications for environmental archives. *Environmental Science & Technology*, *43*(5), 1310–1315. https://doi.org/10.1021/es8029297
Frank, D., Büntgen, U., Böhm, R., Maugeri, M., & Esper, J. (2007). Warmer early instrumental measurements versus colder reconstructed temperatures: Shooting at a moving target. *Quaternary Science Reviews*, *26*(25–28), 3298–3310. https://doi.org/10.1016/j.quascirev.2007.08.002
Franklin, B. (1785). *Meteorological imaginations and conjectures*.
Fritts, H. C. (1976). *Tree rings and climate*. Academic Press.
Gagen, M., McCarroll, D., Loader, N. J., Robertson, I., Jalkanen, R., & Anchukaitis, K. J. (2007). Exorcising the 'segment length curse': Summer temperature reconstruction since AD 1640 using non-detrended stable carbon isotope ratios from pine trees in northern Finland. *The Holocene*, *17*(4), 435. https://doi.org/10.1177/0959683607077012
Gärtner, H., & Schweingruber, F. (2013). *Microscopic Preparation Techniques for Plant Stem Analysis* (Vol. 34, p. 83). Kessel Publishing House.
Gindl, W., Grabner, M., & Wimmer, R. (2000). The influence of temperature on latewood lignin content in treeline Norway spruce compared with maximum density and ring width. *Trees*, *14*(7), 409–414. https://doi.org/10.1007/s004680000057
Grattan, J., & Charman, D. J. (1994). Non-climatic factors and the environmental impact of volcanic volatiles: Implications of the Laki fissure eruption of AD 1783. *The Holocene*, *4*(1), 101–106. https://doi.org/10.1177/095968369400400113
Grattan, J., Durand, M., & Taylor, S. (2003). Illness and elevated human mortality in Europe coincident with the Laki Fissure eruption. *Geological Society, London, Special Publications*, *213*(1), 401–414. https://doi.org/10.1144/GSL.SP.2003.213.01.24
Grattan, J., & Pyatt, F. (1994). Acid damage to vegetation following the Laki fissure eruption in 1783—An historical review. *The Science of the Total Environment*, *151*(3), 241–247. https://doi.org/10.1016/0048-9697(94)90473-1

Grattan, J., & Pyatt, F. (1999). Volcanic eruptions dry fogs and the European palaeoenvironmental record: Localised phenomena or hemispheric impacts? *Global and Planetary Change*, *21*(1–3), 173–179. https://doi.org/10.1016/s0921-8181(99)00013-2

Grattan, J., & Sadler, J. (1999). Regional warming of the lower atmosphere in the wake of volcanic eruptions: The role of the Laki fissure eruption in the hot summer of 1783. *Geological Society, London, Special Publications*, *161*(1), 161–171. https://doi.org/10.1144/gsl.sp.1999.161.01.11

Gu, L., Baldocchi, D. D., Wofsy, S. C., Munger, J. W., Michalsky, J. J., Urbanski, S. P., & Boden, T. A. (2003). Response of a deciduous forest to the Mount Pinatubo eruption: Enhanced photosynthesis. *Science*, *299*(5615), 2035–2038. https://doi.org/10.1126/science.1078366

Gudmundsson, M. T., Thordarson, T., Höskuldsson, Á., Larsen, G., Björnsson, H., Prata, F. J., et al. (2012). Ash generation and distribution from the April-May 2010 eruption of Eyjafjallajökull, Iceland. *Scientific Reports*, *2*(1), 1–12. https://doi.org/10.1038/srep00572

Guillet, S., Corona, C., Stoffel, M., Khodri, M., Lavigne, F., Ortega, P., et al. (2017). Climate response to the Samalas volcanic eruption in 1257 revealed by proxy records. *Nature Geoscience*, *10*(2), 123–128. https://doi.org/10.1038/ngeo2875

Gunnarson, B. E., Linderholm, H. W., & Moberg, A. (2011). Improving a tree-ring reconstruction from west-central Scandinavia: 900 years of warm-season temperatures. *Climate Dynamics*, *36*(1–2), 97–108. https://doi.org/10.1007/s00382-010-0783-5

Hakim, G. J., Emile-Geay, J., Steig, E. J., Noone, D., Anderson, D. M., Tardif, R., et al. (2016). The last millennium climate reanalysis project: Framework and first results. *Journal of Geophysical Research: Atmospheres*, *121*(12), 6745–6764. https://doi.org/10.1002/2016jd024751

Hansell, A., & Oppenheimer, C. (2004). Health hazards from volcanic gases: A systematic literature review. *Archives of Environmental Health: An International Journal*, *59*(12), 628–639. https://doi.org/10.1080/00039890409602947

Hartl, C., George, S. S., Konter, O., Harr, L., Scholz, D., Kirchhefer, A., & Esper, J. (2019). Warfare dendrochronology: Trees witness the deployment of the German battleship Tirpitz in Norway. *Anthropocene*, *27100*, 212. https://doi.org/10.1016/j.ancene.2019.100212

Helama, S., Arppe, L., Uusitalo, J., Holopainen, J., Mäkelä, H. M., Mäkinen, H., et al. (2018). Volcanic dust veils from sixth century tree-ring isotopes linked to reduced irradiance, primary production and human health. *Scientific Reports*, *8*(1), 1–12. https://doi.org/10.1038/s41598-018-19760-w

Hevia, A., Sánchez-Salguero, R., Camarero, J. J., Buras, A., Sangüesa-Barreda, G., Galván, J. D., & Gutiérrez, E. (2018). Towards a better understanding of long-term wood-chemistry variations in old-growth forests: A case study on ancient Pinus uncinata trees from the Pyrenees. *The Science of the Total Environment*, *625*, 220–232. https://doi.org/10.1016/j.scitotenv.2017.12.229

Jones, P. D., Briffa, K. R., & Schweingruber, F. H. (1995). Tree-ring evidence of the widespread effects of explosive volcanic eruptions. *Geophysical Research Letters*, *22*(11), 1333–1336. https://doi.org/10.1029/94gl03113

Knohl, A., & Baldocchi, D. D. (2008). Effects of diffuse radiation on canopy gas exchange processes in a forest ecosystem. *Journal of Geophysical Research: Biogeosciences*, *113*(G2). https://doi.org/10.1029/2007jg000663

Kozlov, V., & Kisternaya, M. (2004). Architectural wooden monuments as a source of information for past environmental changes in Northern Russia. *Palaeogeography, Palaeoclimatology, Palaeoecology*, *209*(1–4), 103–111. https://doi.org/10.1016/j.palaeo.2004.02.006

Kurczyńska, E. U., Dmuchowski, W., Włoch, W., & Bytnerowicz, A. (1997). The influence of air pollutants on needles and stems of Scots pine (*Pinus sylvestris* L.) trees. *Environmental Pollution*, *98*(3), 325–334.

Laufeld, S. (1994). The Lakagígar 1783–84 eruption and its environmental impact in the Nordic countries. *GFF*, *116*(4), 211–214. https://doi.org/10.1080/11035899409546185

Lawrimore, J. H., Menne, M. J., Gleason, B. E., Williams, C. N., Wuertz, D. B., Vose, R. S., & Rennie, J. (2011). An overview of the Global Historical Climatology Network monthly mean temperature data set, version 3. *Journal of Geophysical Research: Atmospheres*, *116*(D19). https://doi.org/10.1029/2011jd016187

Leavitt, S. W., & Long, A. (1982). Evidence for $^{13}C/^{12}C$ fractionation between tree leaves and wood. *Nature*, *298*(5876), 742–744. https://doi.org/10.1038/298742a0

Liang, W., Heinrich, I., Simard, S., Helle, G., Liñán, I. D., & Heinken, T. (2013). Climate signals derived from cell anatomy of Scots pine in NE Germany. *Tree Physiology*, *33*(8), 833–844. https://doi.org/10.1093/treephys/tpt059

Linderholm, H. W., & Gunnarson, B. E. (2019). Were medieval warm-season temperatures in Jämtland, central Scandinavian Mountains, lower than previously estimated? *Dendrochronologia*, *57*, 125607. https://doi.org/10.1016/j.dendro.2019.125607

Loader, N., Young, G., Grudd, H., & McCarroll, D. (2013). Stable carbon isotopes from Torneträsk, northern Sweden provide a millennial length reconstruction of summer sunshine and its relationship to Arctic circulation. *Quaternary Science Reviews*, *62*, 97–113. https://doi.org/10.1016/j.quascirev.2012.11.014

Lükewille, A., & Semb, A. (1997). *Deposition in Norwegian mountain areas*. NILU OR.

Luterbacher, J., Dietrich, D., Xoplaki, E., Grosjean, M., & Wanner, H. (2004). European seasonal and annual temperature variability, trends, and extremes since 1500. *Science*, *303*, 1499–1503. https://doi.org/10.1126/science.1093877

Luterbacher, J., Werner, J. P., Smerdon, J. E., Fernández-Donado, L., González-Rouco, F., Barriopedro, D., et al. (2016). European summer temperatures since Roman times. *Environmental Research Letters*, *11*(2), 024001. https://doi.org/10.1088/1748-9326/11/2/024001

Martin, B., Bytnerowicz, A., & Thorstenson, Y. R. (1988). Effects of air pollutants on the composition of stable carbon isotopes, δ13C, of leaves and wood, and on leaf injury. *Plant Physiology*, *88*(1), 218–223. https://doi.org/10.1104/pp.88.1.218

Mathias, J. M., & Thomas, R. B. (2018). Disentangling the effects of acidic air pollution, atmospheric CO_2, and climate change on recent growth of red spruce trees in the Central Appalachian Mountains. *Global Change Biology*, *24*(9), 3938–3953. https://doi.org/10.1111/gcb.14273

Matisons, R., Gärtner, H., Elferts, D., Kārkliņa, A., Adamovičs, A., & Jansons, A. (2020). Occurrence of 'blue' and 'frost' rings reveal frost sensitivity of eastern Baltic provenances of Scots pine. *Forest Ecology and Management*, *457*(117), 729. https://doi.org/10.1016/j.foreco.2019.117729

Mayer, K., Grabner, M., Rosner, S., Felhofer, M., & Gierlinger, N. (2020). A synoptic view on intra-annual density fluctuations in Abies alba. *Dendrochronologia*, *64*(125), 781. https://doi.org/10.1016/j.dendro.2020.125781

Menne, M. J., Williams, C. N., Gleason, B. E., Rennie, J. J., & Lawrimore, J. H. (2018). The Global Historical Climatology Network monthly temperature dataset, version 4. *Journal of Climate*, *31*(24), 9835–9854. https://doi.org/10.1175/jcli-d-18-0094.1

Mercado, L. M., Bellouin, N., Sitch, S., Boucher, O., Huntingford, C., Wild, M., & Cox, P. M. (2009). Impact of changes in diffuse radiation on the global land carbon sink. *Nature*, *458*(7241), 1014–1017. https://doi.org/10.1038/nature07949

Moberg, A. (2020). *Stockholm historical weather observations—Daily mean air temperatures since 1756*. TEMPS-DAILY-2. https://doi.org/10.17043/STOCKHOLM-HISTORICAL-

Moberg, A., Alexandersson, H., Bergström, H., & Jones, P. D. (2003). Were southern Swedish summer temperatures before 1860 as warm as measured? *International Journal of Climatology*, *23*(12), 1495–1521. https://doi.org/10.1002/joc.945

Morino, K., Minor, R. L., Barron-Gafford, G. A., Brown, P. M., & Hughes, M. K. (2021). Bimodal cambial activity and false-ring formation in conifers under a monsoon climate. *Tree Physiology*. https://doi.org/10.1093/treephys/tpab045

Myśkow, E., Błaś, M., Sobik, M., Godek, M., & Owczarek, P. (2019). The effect of pollutant fog deposition on the wood anatomy of subalpine Norway spruce. *European Journal of Forest Research*, *138*(2), 187–201.

Oman, L., Robock, A., Stenchikov, G. L., Thordarson, T., Koch, D., Shindell, D. T., & Gao, C. C. (2006). Modeling the distribution of the volcanic aerosol cloud from the 1783-1784 Laki eruption. *Journal of Geophysical Research*, *111*(D12). https://doi.org/10.1029/2005jd006899

Oppenheimer, C. (2015). Eruption politics. *Nature Geoscience*, *8*(4), 244–245. https://doi.org/10.1038/ngeo2408

Oppenheimer, C., Orchard, A., Stoffel, M., Newfield, T. P., Guillet, S., Corona, C., et al. (2018). The Eldgjá eruption: Timing, long-range impacts and influence on the Christianisation of Iceland. *Climatic Change*, *147*(3), 369–381. https://doi.org/10.1007/s10584-018-2171-9

Pearson, C. L., Dale, D., Brewer, P., Salzer, M., Lipton, J., & Manning, S. (2009). Dendrochemistry of white mountain bristlecone pines: An investigation via synchrotron radiation scanning X-ray fluorescence microscopy. *Journal of Geophysical Research*, *114*(G1). https://doi.org/10.1029/2008jg000830

Pearson, C. L., Manning, S. W., Coleman, M., & Jarvis, K. (2005). Can tree-ring chemistry reveal absolute dates for past volcanic eruptions? *Journal of Archaeological Science*, *32*(8), 1265–1274. https://doi.org/10.1016/j.jas.2005.03.007

Pearson, C. L., Manning, S. W., Coleman, M., & Jarvis, K. (2006). A dendrochemical study of *Pinus sylvestris* from Siljansfors experimental forest, central Sweden. *Applied Geochemistry*, *21*(10), 1681–1691. https://doi.org/10.1016/j.apgeochem.2006.07.006

Pearson, C. L., Salzer, M., Wacker, L., Brewer, P., Sookdeo, A., & Kuniholm, P. (2020). Securing timelines in the ancient Mediterranean using multiproxy annual tree-ring data. *Proceedings of the National Academy of Sciences*, *117*(15), 8410–8415. https://doi.org/10.1073/pnas.1917445117

Piermattei, A., Crivellaro, A., Carrer, M., & Urbinati, C. (2015). The "blue ring": Anatomy and formation hypothesis of a new tree-ring anomaly in conifers. *Trees*, *29*(2), 613–620. https://doi.org/10.1007/s00468-014-1107-x

Piermattei, A., Crivellaro, A., Krusic, P. J., Esper, J., Vítek, P., Oppenheimer, C., et al. (2020). A millennium-long 'Blue Ring' chronology from the Spanish Pyrenees reveals severe ephemeral summer cooling after volcanic eruptions. *Environmental Research Letters*, *15*(12), 124016. https://doi.org/10.1088/1748-9326/abc120

Prendin, A. L., Petit, G., Carrer, M., Fonti, P., Björklund, J., & von Arx, G. (2017). New research perspectives from a novel approach to quantify tracheid wall thickness. *Tree Physiology*, *37*(7), 976–983. https://doi.org/10.1093/treephys/tpx037

R Core Team. (2019). *R: A language and environment for statistical computing*. R Foundation for Statistical Computing.

Rathgeber, C. B. K., Cuny, H. E., & Fonti, P. (2016). Biological basis of tree-ring formation: A crash course. *Frontiers of Plant Science*, *7*. 734. https://doi.org/10.3389/fpls.2016.00734

Rayback, S. A., Belmecheri, S., Gagen, M. H., Lini, A., Gregory, R., & Jenkins, C. (2020). North American temperate conifer (Tsuga canadensis) reveals a complex physiological response to climatic and anthropogenic stressors. *New Phytologist*, *228*(6), 1781–1795. https://doi.org/10.1111/nph.16811

Robock, A. (2000). Volcanic eruptions and climate. *Review of Geophysics*, *38*, 191–219. https://doi.org/10.1029/1998rg000054

Robock, A. (2005). Cooling following large volcanic eruptions corrected for the effect of diffuse radiation on tree rings. *Geophysical Research Letters*, *32*(6), L06702. https://doi.org/10.1029/2004GL022116

Rocha, E., Gunnarson, B., Kylander, M. E., Augustsson, A., Rindby, A., & Holzkämper, S. (2020). Testing the applicability of dendrochemistry using X-ray fluorescence to trace environmental contamination at a glassworks site. *The Science of the Total Environment*, *720*(137), 429. https://doi.org/10.1016/j.scitotenv.2020.137429

Rohde, R. A., & Hausfather, Z. (2020). The Berkeley Earth land/ocean temperature record. *Earth System Science Data*, *12*(4), 3469–3479. https://doi.org/10.5194/essd-12-3469-2020

Schmidt, A. (2015). Volcanic gas and aerosol hazards from a future Laki-type eruption in Iceland. In *Volcanic hazards, risks and disasters* (pp. 377–397). Elsevier. https://doi.org/10.1016/b978-0-12-396453-3.00015-0

Schmidt, A., Ostro, B., Carslaw, K. S., Wilson, M., Thordarson, T., Mann, G. W., & Simmons, A. J. (2011). Excess mortality in Europe following a future Laki-style Icelandic eruption. *Proceedings of the National Academy of Sciences*, *108*(3815), 715. https://doi.org/10.1073/pnas.1108569108

Schove, D. J. (1954). Summer temperatures and tree-rings in North-Scandinavia AD 1461–1950. *Geografiska Annaler*, *36*(1–2), 40–80. https://doi.org/10.1080/20014422.1954.11880858

Seftigen, K., Linderholm, H. W., Loader, N. J., Liu, Y., & Young, G. H. (2011). The influence of climate on $^{13}C/^{12}C$ and $^{18}O/^{16}O$ ratios in tree ring cellulose of Pinus sylvestris L. growing in the central Scandinavian Mountains. *Chemical Geology*, *286*(3–4), 84–93.

Sheppard, P. R., Ort, M. H., Anderson, K. C., Clynne, M. A., & May, E. M. (2009). Multiple dendrochronological responses to the eruption of Cinder Cone, Lassen volcanic National Park, California. *Dendrochronologia*, *27*(3), 213–221. https://doi.org/10.1016/j.dendro.2009.09.001

Sigl, M., Winstrup, M., McConnell, J. R., Welten, K. C., Plunkett, G., Ludlow, F., et al. (2015). Timing and climate forcing of volcanic eruptions for the past 2,500 years. *Nature*, *523*(7562), 543–549. https://doi.org/10.1038/nature14565

Smith, K. T., Balouet, J. C., & Oudijk, G. (2008). Elemental line scanning of an increment core using EDXRF: From fundamental research to environmental forensics applications. *Dendrochronologia*, *26*(3), 157–163. https://doi.org/10.1016/j.dendro.2008.06.001

Sonnek, K. M., Mårtensson, T., Veibäck, E., Tunved, P., Grahn, H., von Schoenberg, P., et al. (2017). The impacts of a Laki-like eruption on the present Swedish society. *Natural Hazards*, *88*(3), 1565–1590. https://doi.org/10.1007/s11069-017-2933-0

Stoffel, M., Khodri, M., Corona, C., Guillet, S., Poulain, V., Bekki, S., et al. (2015). Estimates of volcanic-induced cooling in the Northern Hemisphere over the past 1,500 years. *Nature Geoscience*, *8*(10), 784–788. https://doi.org/10.1038/ngeo2526

Stothers, R. B. (1996). The great dry fog of 1783. *Climatic Change*, *32*(1), 79–89. https://doi.org/10.1007/bf00141279

Stothers, R. B., & Rampino, M. R. (1983). Volcanic eruptions in the Mediterranean before ad 630 from written and archaeological sources. *Journal of Geophysical Research*, *88*(B8), 6357–6371. https://doi.org/10.1029/jb088ib08p06357

Szeicz, J. M. (1996). White spruce light rings in northwestern Canada. *Arctic and Alpine Research*, *28*(2), 184–189. https://doi.org/10.2307/1551758

Tardif, R., Hakim, G. J., Perkins, W. A., Horlick, K. A., Erb, M. P., Emile-Geay, J., et al. (2019). Last Millennium Reanalysis with an expanded proxy database and seasonal proxy modeling. *Climate of the Past*, *15*(4), 1251–1273. https://doi.org/10.5194/cp-15-1251-2019

Thomas, R. B., Spal, S. E., Smith, K. R., & Nippert, J. B. (2013). Evidence of recovery of Juniperus virginiana trees from sulfur pollution after the Clean Air Act. *Proceedings of the National Academy of Sciences*, *110*(38), 15319–15324. https://doi.org/10.1073/pnas.1308115110

Thorarinsson, S. (1981). Greetings from Iceland: Ash-falls and volcanic aerosols in Scandinavia. *Geografiska Annaler - Series A: Physical Geography*, *63*(3–4), 109–118. https://doi.org/10.1080/04353676.1981.11880024

Thordarson, T., & Larsen, G. (2007). Volcanism in Iceland in historical time: Volcano types, eruption styles and eruptive history. *Journal of Geodynamics*, *43*(1), 118–152. https://doi.org/10.1016/j.jog.2006.09.005

Thordarson, T., & Self, S. (1993). The Laki (Skaftár fires) and Grímsvötn eruptions in 1783–1785. *Bulletin of Volcanology*, *55*(4), 233–263. https://doi.org/10.1007/bf00624353

Thordarson, T., & Self, S. (2003). Atmospheric and environmental effects of the 1783–1784 Laki eruption: A review and reassessment. *Journal of Geophysical Research*, *108*(D1). https://doi.org/10.1029/2001jd002042

Timmreck, C. (2012). Modeling the climatic effects of large explosive volcanic eruptions. *Wiley Interdisciplinary Reviews: Climate Change*, *3*(6), 545–564. https://doi.org/10.1002/wcc.192

Tingley, M. P., & Huybers, P. (2013). Recent temperature extremes at high northern latitudes unprecedented in the past 600 years. *Nature*, *496*(7444), 201–205. https://doi.org/10.1038/nature11969

Tingley, M. P., Stine, A. R., & Huybers, P. (2014). Temperature reconstructions from tree-ring densities overestimate volcanic cooling. *Geophysical Research Letters*, *41*(22), 7838–7845. https://doi.org/10.1002/2014gl061268

Toohey, M., Krüger, K., Schmidt, H., Timmreck, C., Sigl, M., Stoffel, M., & Wilson, R. (2019). Disproportionately strong climate forcing from extratropical explosive volcanic eruptions. *Nature Geoscience*, *12*(2), 100–107. https://doi.org/10.1038/s41561-018-0286-2

Vaganov, E. A. (1990). The tracheidogram method in tree-ring analysis and its application. In E. Cook, & L. Kairiūkštis (Eds.), *Methods of dendrochronology: Applications in the environmental sciences* (pp. 63–75). Kluwer Academic Publishers.

Vaganov, E. A., Hughes, M. K., & Shashkin, A. V. (2006). *Growth Dynamics of Conifer Tree Rings: Images of Past and Future Environments* (Vol. 183). Springer Science & Business Media.

Vejpustková, M., Čihák, T., Samusevich, A., Zeidler, A., Novotnỳ, R., & Šrámek, V. (2017). Interactive effect of extreme climatic event and pollution load on growth and wood anatomy of spruce. *Trees*, *31*(2), 575–586. https://doi.org/10.1007/s00468-016-1491-5

von Arx, G., & Carrer, M. (2014). Roxas—A new tool to build centuries-long tracheid-lumen chronologies in conifers. *Dendrochronologia*, *32*(3), 290–293. https://doi.org/10.1016/j.dendro.2013.12.001

von Arx, G., Crivellaro, A., Prendin, A. L., Čufar, K., & Carrer, M. (2016). Quantitative wood anatomy—Practical guidelines. *Frontiers of Plant Science*, *7*, 781. https://doi.org/10.3389/fpls.2016.00781

Walmsley, J., Urquizo, N., Schemenauer, R., & Bridgman, H. (1970). Modelling of acid deposition in high-elevation fog. *WIT Transactions on Ecology and the Environment*, *14*.

Watanabe, Y., & Ohno, Y. (2020). Severe insect defoliation at different timing affects cell wall formation of tracheids in secondary xylem of Larix kaempferi. *Trees*. 1–11.

Watmough, S. A. (1997). An evaluation of the use of dendrochemical analyses in environmental monitoring. *Environmental Reviews*, *5*(3–4), 181–201. https://doi.org/10.1139/a97-010

Watt, S. F., Pyle, D. M., Mather, T. A., Day, J. A., & Aiuppa, A. (2007). The use of tree-rings and foliage as an archive of volcanogenic cation deposition. *Environmental Pollution*, *148*(1), 48–61. https://doi.org/10.1016/j.envpol.2006.11.007

Wilson, R., Anchukaitis, K., Briffa, K. R., Büntgen, U., Cook, E., D'Arrigo, R., et al. (2016). Last millennium northern hemisphere summer temperatures from tree rings: Part I: The long term context. *Quaternary Science Reviews*, *134*, 1–18. https://doi.org/10.1016/j.quascirev.2015.12.005

Wimmer, R. (2002). Wood anatomical features in tree-rings as indicators of environmental change. *Dendrochronologia*, *20*(1–2), 21–36. https://doi.org/10.1078/1125-7865-00005

Wimmer, R., Strumia, G., & Holawe, F. (2000). Use of false rings in Austrian pine to reconstruct early growing season precipitation. *Canadian Journal of Forest Research*, *30*(11), 1691–1697. https://doi.org/10.1139/x00-095

Witham, C. S., & Oppenheimer, C. (2004). Mortality in England during the 1783–4 Laki Craters eruption. *Bulletin of Volcanology*, *67*(1), 15–26. https://doi.org/10.1007/s00445-004-0357-7

Young, G. H., McCarroll, D., Loader, N. J., Gagen, M. H., Kirchhefer, A. J., & Demmler, J. C. (2012). Changes in atmospheric circulation and the Arctic Oscillation preserved within a millennial length reconstruction of summer cloud cover from northern Fennoscandia. *Climate Dynamics*, *39*(1), 495–507. https://doi.org/10.1007/s00382-011-1246-3

Zambri, B., Robock, A., Mills, M. J., & Schmidt, A. (2019a). Modeling the 1783–1784 Laki eruption in Iceland: 2. Climate impacts. *Journal of Geophysical Research: Atmospheres*, *124*(13), 6770–6790. https://doi.org/10.1029/2018jd029554

Zambri, B., Robock, A., Mills, M. J., & Schmidt, A. (2019b). Modeling the 1783–1784 Laki eruption in Iceland: 1. Aerosol Evolution and global stratospheric circulation impacts. *Journal of Geophysical Research: Atmospheres*, *124*(13), 6750–6769. https://doi.org/10.1029/2018jd029553

Zhang, P., Linderholm, H. W., Gunnarson, B. E., Björklund, J., & Chen, D. (2016). 1200 years of warm-season temperature variability in central Scandinavia inferred from tree-ring density. *Climate of the Past*, *12*(6), 1297–1312. https://doi.org/10.5194/cp-12-1297-2016